This is to certify that the

thesis entitled

Study of Steam Chest Control Valve Failure in Steam Turbines

presented by

Hou Kit Sam

has been accepted towards fulfillment
of the requirements for

MS degree in Mechanical Engineering

Major professor

Date 4/26/01

PLACE IN RETURN BOX to remove this checkout from your record.
TO AVOID FINES return on or before date due.
MAY BE RECALLED with earlier due date if requested.

DATE DUE	DATE DUE	DATE DUE

STUDY OF STEAM CHEST CONTROL VALVES IN STEAM TURBINES

By

Hou Kit Sam

A THESIS

Submitted to
Michigan State University
in partial fulfillment of the requirements
for the degree of

MASTER OF SCIENCE

Department of Mechanical Engineering

2001

ABSTRACT

STUDY OF STEAM CHEST CONTROL VALVE FAILURE IN STEAM TURBINES

By

Hou Kit Sam

Steam turbine control valves are the typical mechanism for regulation of flow into the main turbine itself. However, there has been a long history concerning the failure of the control valves. The failure that the valves experience all seems to be at the same area, which is failure between the valve stem and the top of the valve plug. It also has been theorized that the valve failure is due to fluid-flow induced vibration. This study investigates the valve failure and attempts to recreate the flow through a valve to obtain data points at various positions along the valve plug head as well as the valve seating. The main system studied is a quad-valve system, with the main complication occurring with the middle two valves during their lift action. Current fundamentals of flow theory around valves was considered and integrated with previous research concerning valve failure due to fluid-induced vibration. The actual problem concerning the current valves was then studied and the general causes investigated. Theoretical calculations based on basic theory of fluid-flow induced vibrations were done to obtain an initial theoretical view of the induced vibrations to design an actual experimental setup. Preliminary valve flow calculations were conducted to assist in the design of the experimental testing setup and to predict the possible data that is expected from the actual testing. The primary design concepts for the experimental setup include a single-valve, half-scaled design, with the use of a vacuum pump to induce the flow.

To my family, friends, and the people responsible for my education.

ACKNOWLEDGEMENTS

This research project would not have been made possible without the assistance of Elliot Turbo-machinery Co. in Jeannette, Pennsylvania. The people responsible for their assistance are Naresh Amineni and James Hardin. Their suggestions, questions, and answers have helped guide the general direction of the project and enabled me to move on to each step of the project as quickly as possible.

I would also like to give thanks to my faculty mentor, Dr. Abraham Engeda, who provided me the research project, in seeing the potential of getting the project to a good start. He has also given me direction in the project and allowed me to work with some freedom as to how the project is handled, how the research experimental setup is developed, and in making sure that he and Elliot Turbo-machinery Co. approved the design.

Next, I would like to acknowledge all other professors and friends that have helped me during my stay here in the university, providing me with some help in little bits and pieces, and for being their in helping cope with the stress.

Lastly, I would like to thank my entire family back in Malaysia for providing me infinite support over my college years in helping me with problems that I may have in studying in the Masters program as well as everyday life. I would also like to especially thank Dr. Tom Shih and Dr. Indrek S. Wichman for being part of the final thesis defense and also their time in the classroom for assisting me during the Masters program.

TABLE OF CONTENTS

LIST OF TABLES

LIST OF FIGURES

LIST OF SYMBOLS OR ABBREVIATION

psi	pounds per square inch
pa	Pascal
ft/s	feet per second
m/s	meter per second
in	inch
mm	millimeter
lbs	pounds
N	Newton
Hz	Hertz
d/dt	differentiation
d^2/dt^2	double differentiation
m	mass
C_a	damping coefficients (a is arbitrary denotation)
k_a	spring constant (a is arbitrary denotation)
F_a	force (a is arbitrary denotation)
d	diameter
U	flow of velocity
ρ	density
a	speed of sound
ω	angular vibration frequency
P	pressure
h	valve lift
lb/in^2	pounds per inch square
m^3	meter cubed
ft^3	feet cube
b	throat width
R	cylinder radius
r	radii of curvature
Wq(p)	power spectrum density
x	x-axis displacements
y	y-axis displacements
$\dot{x}$	x-axis velocity
$\dot{y}$	y-axis velocity
$\ddot{x}$	x-axis acceleration
$\ddot{y}$	y-axis acceleration
M_a	sum of the added masses and valve masses (a is arbitrary denotation)
$\dot{m}$	sink flow rate or mass flow rate
g_0	gravitational constant
L	stem length
σ	stress
A	area
V	tangential velocity

D	valve diameter
M_{ang}	momentum change
J	joule
kg	kilogram
K	Kelvin
Btu	British thermal unit
slug	english mass unit
°R	rankine
bar	atmospheric reading
R	gas constant
M	mach number
M^*	mach number at throat
A^*	area at throat
P_0	stagnation pressure
T_0	stagnation temperature
ρ_0	stagnation density
k_a	ratio of specific heats (a is arbitrary denotation)
cfm	cubic feet per minute
acfm	actual cubic feet per minute
scfm	standard cubic feet per minute
BHP	brake horsepower
RPM	revolutions per minute

INTRODUCTION

As the technology for steam turbines progressed, the industry commenced the construction of larger and more powerful steam turbines. However, along with the size and capacity increase, more importance was also stressed in the regulation of the flow by the control valves. Based on the rotational speeds or loading signals, the control valves regulate the amount of flow through the turbine to control the output. The turbine that is being investigated possesses a four-valve system. There has been a long history regarding the reliability of these control valves. Even with four valves, operations at such high temperatures and pressures and vast pressure differences between the inlet and outlet of the turbine will subject the valve to enormous dynamic and static hydraulic forces and subjects the valves to abnormal vibrations. This research project's objective is to take an in-depth look and to determine if it is indeed the fluid-flow induced vibrations that cause failure of the valves. The failure of the control valves in this turbine under study occurs in two of the four valves, the two center ones to be specific. An initial theoretical study of fluid-flow induced vibrations was made and a brief history of the most recent study on similar valve failures was also conducted to provide a direction towards the best method to tackle this problem. It was then decided that a single valve, half-scale model would be adequate, designed to minimize cost of construction, and calculated to be adequate in terms of data collection. The half-scale size is slightly more than enough to position and fit in the necessary static and dynamic pressure gauges. Once the data is analyzed, a more in-depth realistic view of the valve flow can be made. It is hoped that this research will help provide a more definitive look on valve failure.

CHAPTER 1
The Current Research of Quad-Valve System Failure

1. Current Research with Control Valves

The problem that is currently being studied involves a quad-valve system that controls the steam flow into the turbine. The steam chest operates at about 1600 psi (11 Mpa) and with fully lifted valves; the pressure drop is at about 100 psi (0.69 Mpa).

With valve flow operating at a choked flow, which is approximately about 2000 ft/s (609.6 m/s) at a valve lift of about 0.7 in (17.78 mm), an increase of steam pressure causes the number 2 valve to fail due to severe vibrations. From a closer physical analysis and simple initial failure analysis, it was determined that the valve experiences an extremely high lateral vibration at that valve lift position. An axial force of about 3200 lbs (14234 N) is estimated to be experienced at this lift. The number 2 valve, which is one of the problem valves that have been tested, with an infinitely stiff support, has a high lateral, or bending, resonance of 600Hz, and as the support stiffness reduces, the resonance are found to be as low as 350Hz.

The Mach number, pressures, and flow velocities of the actual valve have been mapped out with two lift positions that experience the instability and vibration most commonly. The main problem occurs during the valve wide-open lift, which is at 0.639 inches. The other lift, at 0.4595 inches, experiences the same type of vibrations and instability, although not as intense in magnitude. For comparison purposes, and to observe the apparent increase in the undesirable effects of instability and vibration, the profiles for the 0.4595-inch lift is shown first, followed by the 0.639-inch lifts. Patterns for the Mach number, pressure and velocities change as the lift increases. These profiles can be found in Appendix A.

Two causes for the unusual vibration have been identified. The first cause, which is more specific, deals with the acoustic inlet resonance in the steam chest box. The second cause, involves the flow-induced forces that cause the lateral vibration and instability. With high-speed flows in the operation of the turbine, both the acoustic environment and the mechanical resonant characteristics of the valve will be adversely affected.

1.1 Acoustic Resonance

The method to check acoustic resonance is to use finite element modeling. The steam flows are what is usually modeled. The natural frequencies of the flow path are determined using a 3-D model using a standard value for the speed of sound. Additional analysis was used with variations of the speed of sound value by roughly 10 percent. Scaling these frequency values can be done for any pressure and temperature because these natural frequencies are linearly proportional to the speed of sound.

Downstream Flow Paths	Outer Channel		Inner Channel	
	1st Mode	2nd Mode	1st Mode	2nd Mode
2000 ft/s	337.8	558.7	428.9	744.5
Zero Impedance at End	337.8	558.7		
2200 ft/s	371.6	614.6	471.8	818.9
1800 ft/s	304.0	502.8	386.0	670.0
Using a Finer Mesh	337.6	552.5	427.1	744.7
Theoretical Hollow Cylinder of Same Length	333.0		460.0	

Table 1. Acoustic Natural Frequency Values Found with Finite Element Analysis

From the table above, we see the various natural frequencies at various speeds and modes in the outer and inner channels. The interior nozzles have a first mode frequency of 558 Hz when the speed is at 2000 ft/s. However, in order to have a lower frequency at this mode, the speed of sound was found to be lower for this to occur. With a 350 Hz mode found in the outer nozzles and not in the inner nozzles, the acoustic response of the nozzles is not the contributors to the actual valve vibrations. This conclusion can be further confirmed with the fact that the valves vibrate laterally, while the acoustic modes is a longitudinal mode, with very little lateral components.

1.2 Flow-Induced Valve Instability

This has been most probably the leading cause of vibrations in the lateral direction. Although a summary of how this affects the valve has been given, a further account for its contribution to the actual research problem at hand will be mentioned here.

The flow-induced instability is usually velocity dependent, density dependent and is highly dependent on the flow geometry. Other factors that can be included that contribute to the instability are the local acoustic modes and the mechanical resonance. Increasing pressure operation in the steam chest has been observed to create higher vibrations. Changes in stem stiffness also contribute to the instability of the valves. With an offset valve lift, or valve eccentricity, which will be explained later, the flow velocity on the side with the smaller flow area will increase, and the flow in the larger flow area will decrease. The lower velocity area will tend to have an increase in local pressure, resulting in a net force developed. This force will cause a bending moment on the valve and a bending stress. And once the force bends the valve the other direction, it will close the flow area on the other side and the development of the force will occur on the other side and bend the valve the opposite direction. This is the vibrational characteristic of this lateral bending in the valve. The phase of these forces to the valve inertial, stiffness and damping forces are the important components to developing the large amplitude responses. The flow-induced vibrations involving such mechanical responses to the flow as mentioned above are typical of one of three categories.

1) Forced responses can occur when the valve structure responds to the flow forces. The structural motion does not really influence the basic characteristics of the fluid forces. For this particular problem, the transition from choked flow to normal flow could generate unsteady non-symmetrical forces, which could possibly be responsible for the strong lateral vibrations.
2) Some divergent instability can occur during stiffness-dominated events in structure and fluid interactions, which causes the structural responses to be small, until it meets some critical threshold. This critical threshold is when the structure's response turns divergent. This divergence can be limited however and when it does, it may appear with an oscillatory characteristic.
3) With the presence of an oscillatory instability, this response can increase in magnitude when the mechanical damping is negated by the interaction of the valve structure and the fluid flow.

The second and third categories are mechanisms of self-excited vibrations. The amplitude responses to these mechanisms are usually large and extreme, which can lead to failure in short periods of time. Both these mechanisms do not require a periodicity in the flow for the instability to occur and to have the response to occur.

With many factors that can trigger the instability of the valve, it is extremely hard to determine which are the outstanding factors that contribute to the valve failure. However, a simple forced response cannot really be identified as the sole cause. Since many factors are involved in studying these vibrations, scale modeling and testing is the most reliable method of studying this problem.

CHAPTER 2
Fundamentals and Flow Theory of Control Valves

1. Brief Fundamentals of Venturi Control Valves

Valves are used to regulate the flow of the fluid into a turbine in a very accurate and precise manner. Secondary functions of valves include control valves that are speed-responsive to control flow through the turbine, emergency valves to prevent uncontrolled over-speeding, and auxiliary functions such as steam-seal-regulator pressure control of gland seal steam. Various types of valves are used for all these functions. This research concerns with inlet control valves of a venturi type. The venturi type valves are used because of their low wide-open pressure drop and high flow coefficient to permit the use of smaller sized valves to pass a given flow. Valve-contact diameter is used to calculate the valve unbalance against which the steam unbalance pressure will react. The actuators that control these valves must be able to tolerate and lift the valve against this force. The valve disk is a hemisphere with a short, conical seat so that when the valve is closed, there is total line contact and no flow can penetrate. Figure 1 shows the typical venturi valve design.

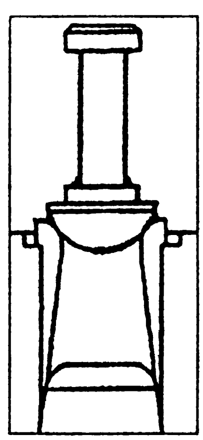

Figure 1: Venturi Valve

The valves are usually located within a pressure chest, and they are positioned in response to signals from the overall control system so that the flow can be controlled to produce the amount of power to correspond to the load at the desired frequency or speed. Therefore, regardless of the size of the turbine, the control valves must be able to withstand pressures of all magnitudes, and must be able to tolerate all forms of valve lifts, from just barely opened to wide-open positions. Control valves must also maintain the thermal efficiency of the steam turbine in operation, and higher pressure drops yield lower thermal efficiencies. Thus it is important to maintain low pressure drops within a turbine. Substantial pressure drops can be done without much loss of thermal efficiency through a multiple control valve system. The programming of the valves is such that only one valve is lifted in a certain sequence at time, while the other valves are at a lift that provides a minimum pressure drop. It is also important that the flow through the valve should be proportional to the lift of the valve because the power output of the steam turbine is also influenced by the valve flow characteristics. If this proportionality can be made into a linear relationship, then the turbine output can also be made into a linear relationship. This is the ideal relationship for the control valves, and design of the control system should be made so that this proportionality is achieved. For the multi-valve system, the correct sequence must be configured so that this proportionality is observed. In reality, this does not occur exactly, but the linear relationship can be closely replicated, and it can only be done at a valve lift range of 0 to 20 percent. Turbine power output will change at a more drastic rate between valve lift ranges of a smaller increment than a lift range of a larger increment. Larger power increment at a smaller lift change is known as a steep flow travel curve, and the smaller power increment at a larger lift range is known as a flat spot. Below is a simple graph that shows 2 turbines that operate in conjunction, with one turbine operating on the steep flow travel curve, and the other on the flat spot.

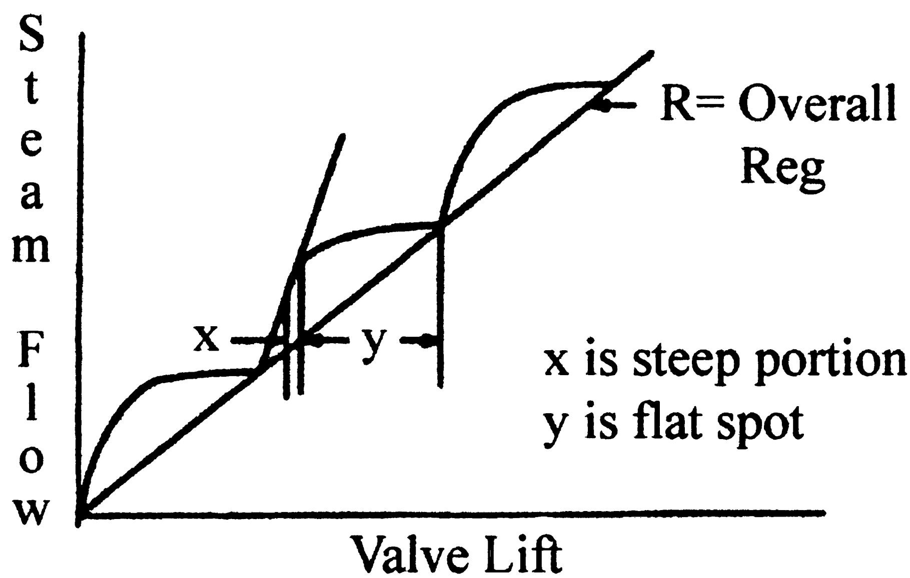

Figure 2: Relation Between Steam Flow and Valve Lift
(Source: Installation and Service Engineering Training Manual: Version 2.1)

Notice that the turbine operating on the steep flow travel curve will take almost all of the load change, while the one with the flat top operation will take almost no load at all. Both cases are not the most satisfactory operating conditions. Depending on the desired operating conditions, changing the shape of valves and/or seating would change the relationship of the steam flow. The other method would be to alter the valve lift timing and sequence of valve operation.

2. Fluid Forces in Control Valves

In order to study the problem and to observe their behavior in the research, a brief understanding of the fluid forces involved in control valve flow must be established. It has been traced that fluid flow problems have occurred on the moving parts of the plug of the valve due to fluid forces. In properly understanding the forces involved, phenomena during the experimental testing can be identified and observed. There have been 11 different types of fluid reaction that have been observed and identified. These forces are observed in the moving parts of the valve, in this case the plug of the valve. After this section, it can be seen that most service limitations of control valves are dependent on pressure differences. Limiting valve body velocity has been seen as a universal remedy for valve failure, and the limitation of hydraulic power or mass velocity as another, but it's the pressure drop that is the measure of the magnitude of the valve failure problem, which in turn is the limiting condition for the operation of a turbine.

2.1 Problems with Valve Travel

During the closed position of a plug valve, the action of fluid forces is minimal, even when there is a high pressure increment across the valve. Pressures on the plug commence variation with fluid momentum and pressure losses as the valve lift increases. This results in a varying vertical force along different positions of the plug head, and this may exceed the force that is observed when the plug is in the closed position. With the selection of an actuator based on a zero-lift unbalance, the valve would stroke less than the specified signal span. But, if the full-lift force is of a tensile nature, a full valve lift might be smaller than expected. Below is a graph that describes the relationship between the plug force and the valve lift in a balanced valve. As the valve lifts, this force decreases, even becoming tensile for a bit before the fluid exerts a larger vertical force on the moving plug.

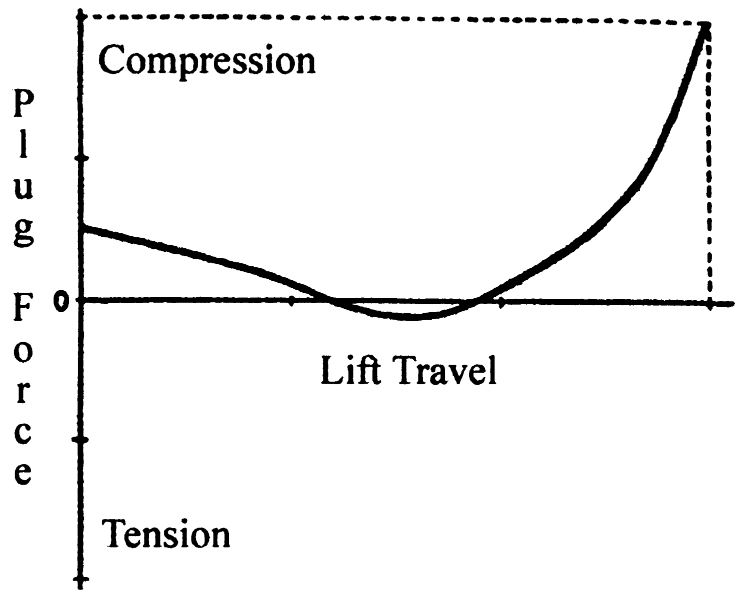

Figure 3: Balanced Valve Lift Correlation with Plug Force.
(Source: Understanding Fluid Forces in Control Valves, May 1971)

For an unbalanced valve, more complications will arise, as described above. This is summarized in the figure below.

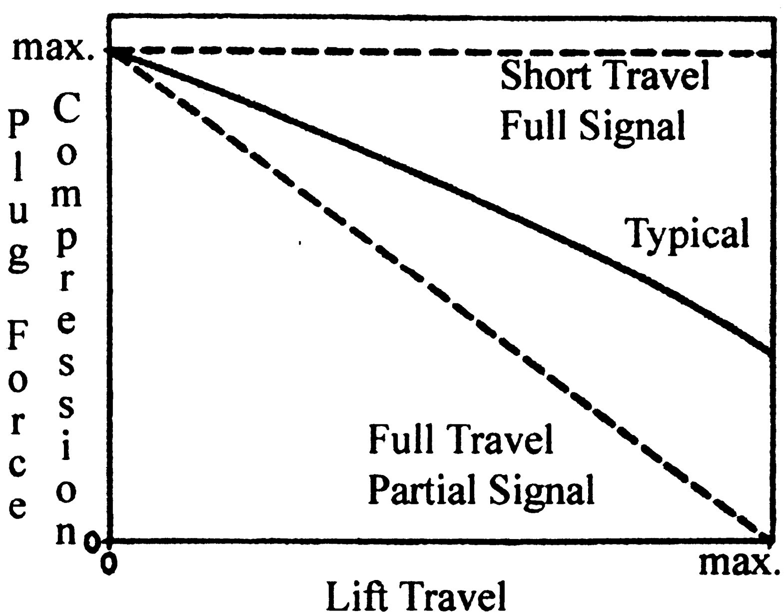

Figure 4: Unbalanced Valve Lift Correlation with Plug Force.
(Source: Understanding Fluid Forces in Control Valves, May 1971)

Figure 4 shows that maximum compressive force occurs at zero lift. During unbalanced to zero-lift, full travel either will not occur or it will occur with only a partial signal span.

Since a portion of the plug force is a direct function of the pressure drop across a control volume around the plug, it is essential that the force on the plug be known if the valve is going to work with the intended valve lift, given the required signal span. Much of the force is related to variations in fluid momentum and thus is proportional to mass-velocity changes. It has been shown that fluid-momentum forces are directly proportional to the pressure drop and independent of other service limitations, such as flow velocity or hydraulic power.

In summary, many have speculated that once the force crosses the zero plug force line in figure 1, it stands as a potential area where valve instability occurs. However, there is no solid evidence to prove this, and sometimes can be neglected in an analysis of valve plug forces.

2.2 Large Side Loadings and Excessive Torque

With the theory that vertical forces on the valve are a direct proportion to pressure change also apply to forces that are perpendicular to the valve, which are found applied to the stem. Even with the established pressure change as the governing criteria, it is still difficult to choose certain values for it to result in a clean, good operation. Temperature and materials composition further complicate the selection of values of pressure change. Side loadings can still be determined as a function of pressure change, and still be just a function of pressure change, and independent of flow velocity or hydraulic power.

As for torque effects, it has been shown that they are also dependent on pressure drops, but their effects are very uncommon. This is probably due to poor wing guiding of the plug, which limits the plug to just low pressure uses.

2.3 Vertical Buffeting and Horizontal Vibrations

This is the phenomenon that has contributed to many valve failures over the years. Figure 3 in the previous section show only a balanced valve lift correlation with vertical force when only the steady-state component of the vertical force is mapped. The figure below shows the actual relation in reality.

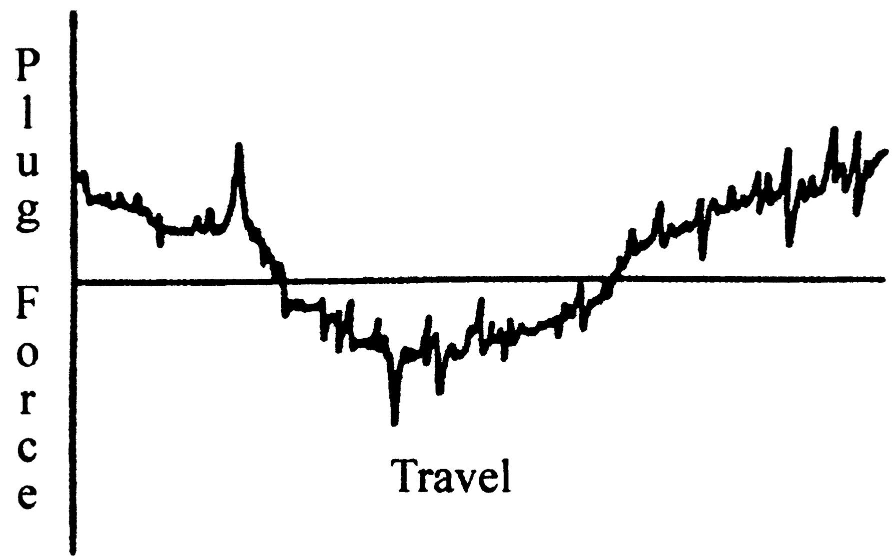

Figure 5: Reality Correlation with the Valve Lift and the Vertical Forces.
(Source: Understanding Fluid Forces in Control Valves, May 1971)

This graph is a general result of test data with real time-varying vertical forces. As it is shown, buffeting occurs due to the time-varying component. A flat force spectrum can be seen in a range of frequency from 0 to 100 Hz. This however, may develop peak-to-peak force values exceeding 1000 lbs. Buffeting forces are proportional to pressure drops while the resisting forces are related to the system's friction and possible actuator stiffness. Because of this, calculation and prediction of buffeting can be done, and therefore can be avoided by using appropriate pressure drop limits. Depending on the magnitude of the frequency of buffeting forces, they can extend into the realm of the ultrasonic, with the forces acting in almost all directions and planes. Moving parts that resonate in a certain directions give rise to complications. Resonance of the moving parts at its natural frequency, such as the valve stem and plug, results in noise, parts heating, and eventual failure. At high frequencies, this problem may not be isolated to just the pressure change, but a more complicated function of pressure change as well as valve aerodynamic noise generation.

Vibration, a horizontal form of buffeting, is probably the most common form of buffeting. The time-varying forces involved in vibration are still a function of pressure change, but unlike vertical buffeting, their prediction and solutions are often difficult to investigate, at least in the lower frequency ranges. Certain types of valves vibrate at lower frequencies, so sometimes their vibration characteristics are somewhat predictable, with the basis as a function of pressure change. However, other types of valves have the vibrational characteristics complicated with buffeting forces cause by secondary flow paths and by stabilizing effects of steady-state lateral forces. During experimental tests, results from repeated tests provide different data, making a conclusion for a general relationship describing vibrations a complex task. At higher pressure drops, vibrations are even harder to predict, and are usually not satisfactory if they are made with some solutions although some progress is being made.

2.4 Bi-stable Action from Negative Gradients

This means a variety of problems that occur when the valve/actuator system is unable to maintain a fixed position along its travel range. The cause of this problem has been identified as a negative fluid force gradient. This gradient exists in any valve which has movement of the plug resulting in a change in fluid force which will lead to the movement of the plug in the same direction, whether its lifting or closing. For a configuration in which the actuator is above the valve, a negative gradient will exist on 2 occasions. The first is the "Push-down-to-close valve", in which the force curve shows decreasing tension as the valve opens. The other is the "Push-down-to-open valve" situation, in which the force curve shows increasing tension as the valve opens.

Force curves are derived with a constant pressure change, and then extrapolated by the proportional relationship between pressure change and force. In order for a problem to be completely predicted with a solution, the maximum negative gradient must be calculated. Taking the slope of the constant pressure change force curve does this.

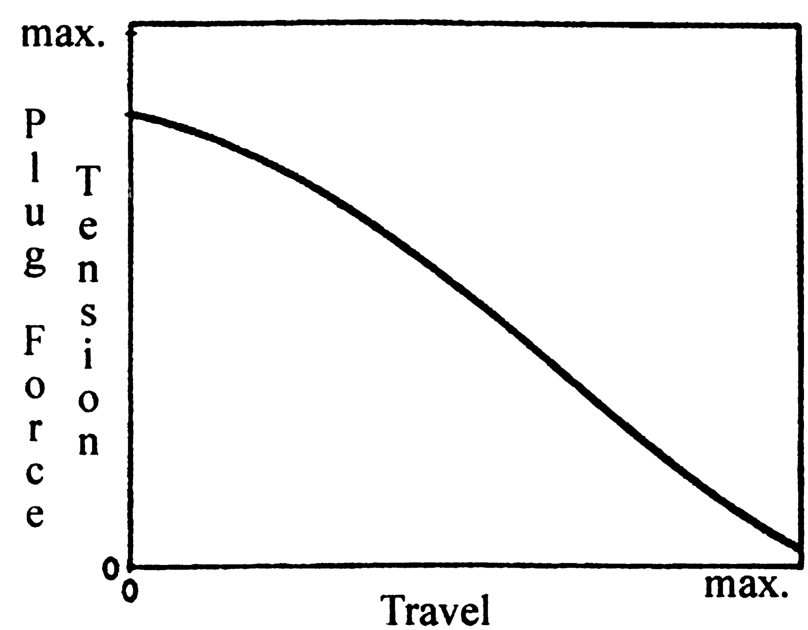

Figure 6: Force Curve of Unbalanced Valve Design.
(Source: Understanding Fluid Forces in Control Valves, May 1971)

This design is bi-stable, with a fixed position only occurring in the fully open or closed position. A negative force gradient is seen here, which shifts the plug off its assigned position. With a constant actuator force being applied, the plug goes to full open position, since less tensile force is required to keep it opening. Similarly, when the valve is closing, The actuator still applies a constant force, but more tensile force is required to keep it closing, so the valve goes to full closed position.

In reality, when constructing a constant pressure change force curve, the data can be extrapolated directly. However, with the plug movement affecting the differential, the gradient must be reconstructed to regard the steady state and transient differentials. This results in a more severe negative gradient that is found, or installed, on an inherent negative gradient. Therefore, it is not uncommon to find an installed negative gradient force curve on a valve/actuator design that has either no inherent negative gradient or a positive gradient. Valves with a "push-down-to-close valve" design operating with a stem in tension and valves with a "push-down-to-open valve" design with a stem in compression will generally have this phenomenon present.

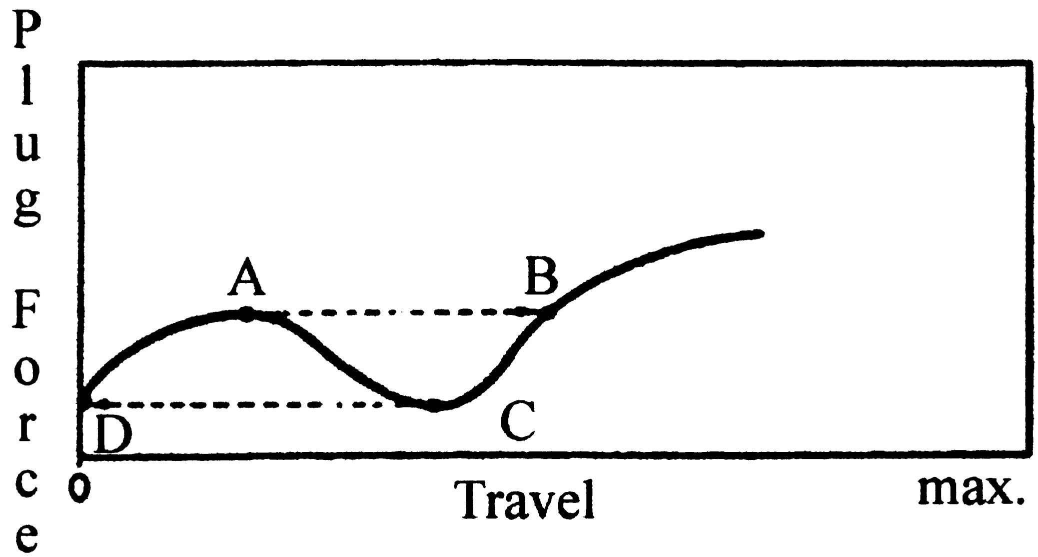

Figure 7: Force Curve of Balanced Valve.
(Source: Understanding Fluid Forces in Control Valves, May 1971)

Bi-stable plug action can still be present in this valve design shown in figure 7. Change in actuator force will stroke the valve to point A, and a further force change in the same direction will satisfy the force requirements for point B and the valve will jump over to that position. If the actuator reverses the direction of the force, the plug will move slowly back to point C, but will then jump over to position D. It's during these jumps that there is bi-stabilization and thus the presence of a negative force gradient.

With the existence of these negative gradients from cases described above, the closed-loop oscillation frequency can vary from a low operating frequency to a maximum at the natural frequency of the valve/actuator spring mass system. The only solution for the negative gradient in this case is to provide an actuator with a positive gradient that exceeds the negative gradient. Some valve designs are substantially well balanced for steady-state conditions, which involve low plug velocity, but can still possess a negative gradient during a high-speed operation. In this case, a common solution is plug redesign or a stiffer actuator. A solution for all valve type designs would be to limit the plug stroking speed for small actuator signals while still allowing high stroking speeds for large signals.

2.5 Emergence of Unpredictable Vortexes

Tests from laboratories have described the phenomenon as a product of 2 distinct flows that occur at the same valve position and pressure drop. These unpredictable vortexes are found in almost all valve types, but are more prominent in flow-close angle valves. In a closed loop system the problem shows up as a low frequency cycle. Some reactions occur during the flow switching but this low frequency cycle is dominated by flow changes rather than force changes. If these vortexes are found during low plug lifts, the problem can be solved or minimized by valve trimming. However, if higher lifts are required for the valve system, then the best solution is to apply an anti-vortex web.

2.6 Complications from a Minor Loop Cycle in the Process System

Most of the control valve problems described above are part of the major loop cycle, which involves the actuator, the valve, process, transmitter and controller. An important minor loop cycle is formed by process pressure feedback to the summing point of the valve plug force. Negative gradients cause a positive feedback, or even a negative feedback where there is a significant time lag in the process. This may lead to difficulties, as the cycle will occur at the plug/actuator natural frequency if loop gain is high. This problem can be solve by inserting a higher rate spring or increased damper, but if the damping is obtained by way of friction, then this solution may cause deterioration in the steady-state performance.

2.7 Complications from Cavitation, Noise, Erosion, and Compressibility

Although it has been identified that the pressure change is the significant service condition to base all functions of force, the question arises as to which pressure change should be used. Since mass flow rate contributes much to the overall force of a valve system, it has to be decided whether the total pressure change be used, or the pressure change that only produces the mass flow rate changes. The decision is made based on the significance that the 2 types of pressure changes have to the forces. If the mass flow rate forces are more dominant, then the pressure change that affects the change in mass flow rate should be used, but only in this case. All other cases it is much more appropriate to use the total pressure change. If the flow forces reach a maximum when the outlet pressure is decreased such that choked flow occurs, then it is better to use the total pressure change. This applies to tests that involve buffeting. For large loadings, excessive torques and horizontal vibrations, the total pressure change is also used. The same applies for vertical forces on the stem and pressure forces near the valve seating. At higher lifts, the mass flow rate forces start to dominate, and another variable is used to assist in the prediction and calculation. This new variable is usually the pressure ratio.

Cavitation also uses the pressure change as the dominant service condition. Noise, however, has another variable that is used, which is the body outlet velocity. Noise is a rather complicated problem and prediction and solutions cannot be achieved as simply as other phenomenon which used pressure change as the dominant variable. Erosion is also another complex phenomenon, which involves many variables, including body velocity. However, it is not enough to have simple guidelines constructed for prediction and solutions, as with the other problems mentioned in previous sections. There is no simple limit to establish on the fluid flow that will cause erosion of the material of the valve or seating to be set to a minimum or non-existent amount. Therefore, a much more complicated study is being ensued to solve this problem.

CHAPTER 3
Previous Research and Testing of Fluid-Induced Vibration

1. Description of Fluid Vibrations with Vibrational Model of Control Valve

Looking at the valve system, it is clear that the long valve stem might be susceptible to vibrations. The primary directions for the vibration are in the longitudinal direction as well as the horizontal direction, or bending direction. This valve can be modeled in the 2 directions, the horizontal and longitudinal directions, much like spring-mass system as shown in the figure below.

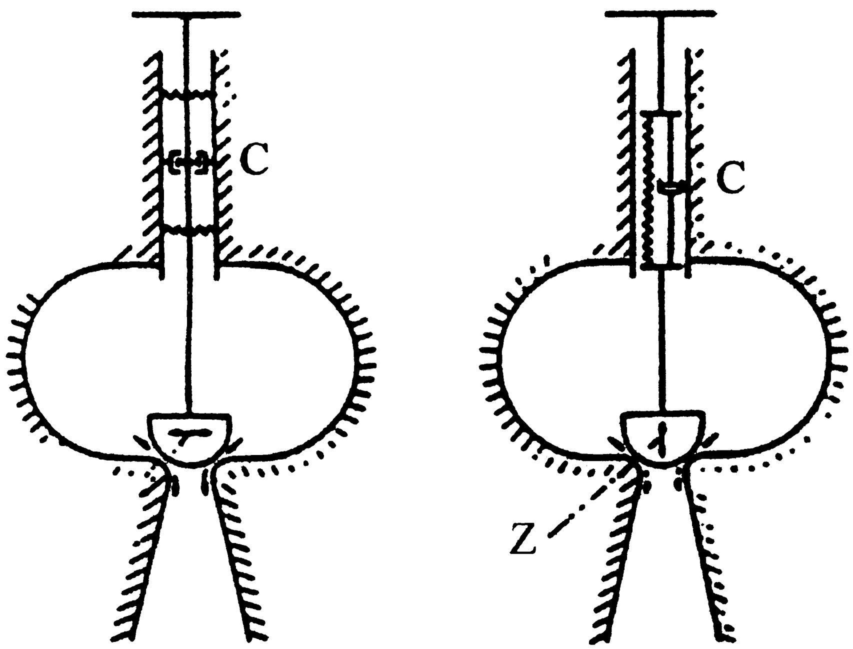

Figure 8: Vibration Model.
(Source:Fluid Induced Vibration of Steam Control Valves UDC 534.11.001.5:621.165-3)

The following equations of motion for the models shown in figure 8 are shown below as equations 1 and 2.

$$m\frac{d^2x}{dt^2}+C_B\frac{dx}{dt}+k_Bx=F_x \quad (1)$$

$$m\frac{d^2z}{dt^2}+C_v\frac{dz}{dt}+k_vz=F_z \tag{2}$$

where m is the mass, C_B and C_v are the lateral and longitudinal damping coefficients, k_B and k_v are the lateral and longitudinal spring constants, and x and z are in the lateral and longitudinal displacements respectively. F_x and F_z are the directional forces in the x and z directions respectively. Although these models do not reflect the real actions of the valve, a simple linearization of the problem can be made with this model to estimate and explain the measurement results with the real valve behavior in the actual turbine.

To describe the variables responsible to calculate the forces in the horizontal and vertical directions, we see below the forces expressed as a function of these variables. Note that the variables are of the dimensionless form.

$$Fx, Fz = \frac{xD^2}{4}(P_{in}-P_{out})f\left[\frac{U}{a},\frac{Uh\rho_2}{\mu_2},\frac{\omega D}{U},\frac{P_{out}}{P_{in}},\frac{h}{D}\right]$$

where D is the diameter of the valve opening, U is the flow of the velocity, ρ is the density, a is the speed of sound, ω is the angular vibration frequency of the valve, and P is the pressure. Looking at the dimensionless variables, some can be related to well-known dimensionless numbers. The first in the brackets is the Mach number, and the following ones are, in order, the Reynolds number, a dimensionless frequency term, pressure ratio, and a valve-opening ratio. As in the previous section, the limiting condition for the prediction and solution for vibrational force is the pressure change, which is seen here.

For this model, there is also the assumption that there are compelling forces present, namely damping and restoration forces, that are found to vibrate with the pressure fluctuations whish are proportional to the velocity of the valve vibration. The amplitude of these vibrations can be expressed by variables and are found in the x and z directions. Their relationships are shown below.

$$x' = f\left[\sqrt{\frac{k_B}{m}}t, \frac{C_B}{\sqrt{mk_B}}, \frac{D(P_{in} - P_{out})f}{k_B}\right]$$

$$z' = f\left[\sqrt{\frac{k_v}{m}}t, \frac{C_v}{\sqrt{mk_v}}, \frac{D(P_{in} - P_{out})f}{k_v}\right]$$

Equations that are defined by these 3 variables, in a sense are extremely powerful. This is because if the 3 variables are made such that they correspond to those of the actual turbine when simulating the actual turbine with a model, these 3 variables can be directly determined. The first 2 variables in the brackets are determined by examining the valve structure, while the hydraulic force due to the flow around the valve structure determines the last one, which is also considered a spring constant ratio. The value f is determined by hydrodynamic parameters shown with the equations above.

Looking at the correlation of the equations above, it can be seen that if the pressure change in the turbine is very high, the Reynolds number is also very high. Reynolds numbers can be calculated based on representative dimensions of valve lift, representative velocity of flow rate, and another representative dimension of valve diameter. However, since it is impossible that the predicted Reynolds number is the same as the actual one, the relations above is somewhat tweaked, such that the dependency of the Reynolds number is small in the flow through the valve. Thus the Reynolds number will not be the determining factor in the prediction and solution for this research.

2. Previous Research for a Two-Dimensional Test

This section describes the method and some tests results regarding an experiment that was conducted on a previous research, based on a two-dimensional model. It will describe some simple models and data acquisition methods to obtain some data results.

2.1 The Two-Dimensional Model Test

In order to determine the flowing pattern within the valve system, a two-dimensional, transparent model of the valve is used, so as to obtain an initial observation of the flow. With a two-dimensional model, the valve structure makes the valve impossible to vibrate in the parallel direction. This makes the natural frequency of the valve very high, and thus it can be assumed that the valve is a rigid body. Thus influence of the valve vibration on the fluid can be neglected. The inlet pressure that was used was about 24 Mpa (3480 lb/in.^{2}) at the valve inlet and about 0.005 Mpa (0.725 ib/in.^{2}) at the valve outlet. This gave a pressure ratio of about 0.00021, with a supersonic flow velocity. With a higher valve lift, the pressure ratio will eventually get larger and the valve flow will get slower. Through this range of pressure ratio we have to observe the change of flow patterns. The model constructed was also scaled down to 1/3 of the actual size.

The main apparatus used in this previous research test was a wind tunnel with the capability of a blow down. A main reservoir tank with a capacity of 45 m^3 (1590 ft^3) with a pressure of 3 Mpa (427 lb/in.^{2}) is used to flow through a control valve into a surge tank with a capacity of 10 m^3 (353 ft^3). The model valve is then connected to the outlet of the surge tank via another control valve. To ensure that turbulence and non-uniform inflow wasn't a factor in the data, the passage before the inlet of the model valve was made adequately large so that the velocity was reduced to a point that laminar flow was still present. This also makes the pressure ratio between the inlet and outlet of the model valve maintained.

Since looking at the flow was the main priority in this test, the valve was made so that the aspect ratio between the valve width and depth exceeded a value of 2. Static and dynamic pressure gages were positioned with 5 around the valve, 2 in the valve wake flow diffuser area, and 2 at the valve inlet. The overall testing setup is shown below.

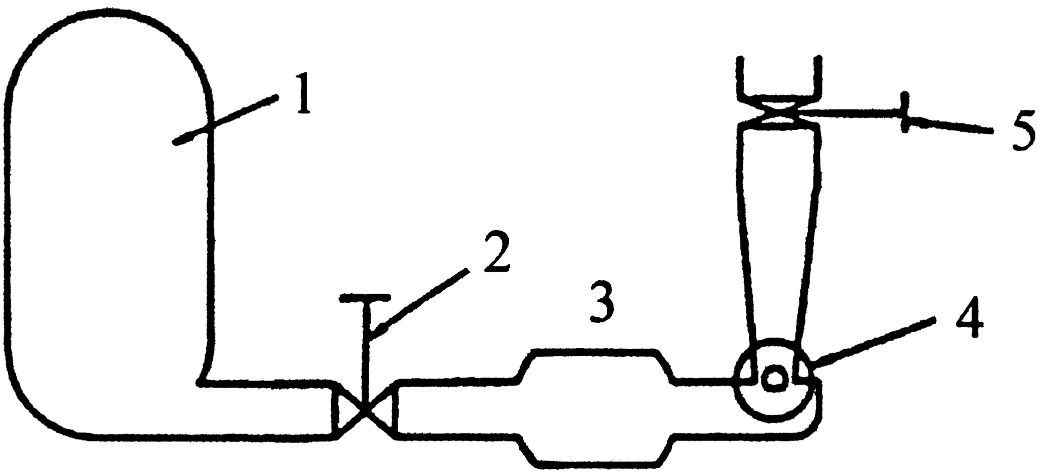

Figure 9: Experimental Testing Setup to Observe Two-Dimensional Flow through a Valve System
(Source:Fluid Induced Vibration of Steam Control Valves UDC 534.11.001.5:621.165-3)

2.2 The Results and Observations of the Two-Dimensional Test

The main objective of the two-dimensional test was to observe the flow through the valve. At any pressure ratio, the test resulted in a two-dimensional free jet flow, without a random wake or a turbulent flow vortex, which will be observed once the three-dimensional flow test is examined. The pressure ratio affects the shape of the flow through the valve and valve seating. At high pressure ratios, the jet flow through the valve on one side seems to stick with the valve up to the point near the center of the valve, while the other jet flow on the other side is free flowing and flows downstream. Both jet streams in this case are right-left asymmetric, and are shown in figure 10.

Figure 10: Flow through the Valve at a High Pressure Ratio.
(Source:Fluid Induced Vibration of Steam Control Valves UDC 534.11.001.5:621.165-3)

With a small pressure ratio, the flow on both sides are free-flow jet streams, and are both right-left symmetrical which join together after flowing past the valve. This phenomenon is shown in figure 11.

Figure 11: Flow through the Valve at a Low Pressure Ratio.
(Source:Fluid Induced Vibration of Steam Control Valves UDC 534.11.001.5:621.165-3)

This sort of flow can be simulated by having a flow between 2 cylinder columns, but only if the area of flow observed does not include the effect of right and left flows joining together in the wake flow. Considering 2 different sized cylinder columns, with a large pressure ratio, the flow was found to adhere to the cylinder of larger radius of curvature. A small pressure ratio yields the flow moving away from both cylinders, and thus a free jet flow is observed.

Looking at both the flows through the model valve and the flow pattern, it was concluded that the flow behavior at high or low pressure ratios is the result of non-steady state flow patterns. These flow patterns occur by turns at irregular intervals in the transient flow area. The pressure corresponding to these flow patterns also change in sync by turns of irregular intervals on the wall surface of the valve and valve seat. With the free jet flow produced with a small pressure ratio, the jet stream itself vibrates and possesses a pressure variation spectrum vibrating at a peak frequency. If the pressure ratio is large, the jet stream is randomly patterned, with the randomness decreasing as the frequency of the spectrum increases. In correlation to the test results of the valve experiment, the non-steady state flow does not occur except at the boundary where the pattern of flow changes and at small pressure ratios where the flow is a free jet. Great pressure variations occur as the flow becomes unstable, and to prevent this from occurring during high pressures, the flow must adhere to the valve or the flow pattern must change without undergoing the unstable state. From further examination of the results from the flow through the 2 cylinder columns, the unstable area is a function of the ratio of the throat width b to the radius of curvature of the 2 cylinders R, and the ratio of radii of curvature of the two cylinders r/R. The figure below shows the relationship between the 2 ratios.

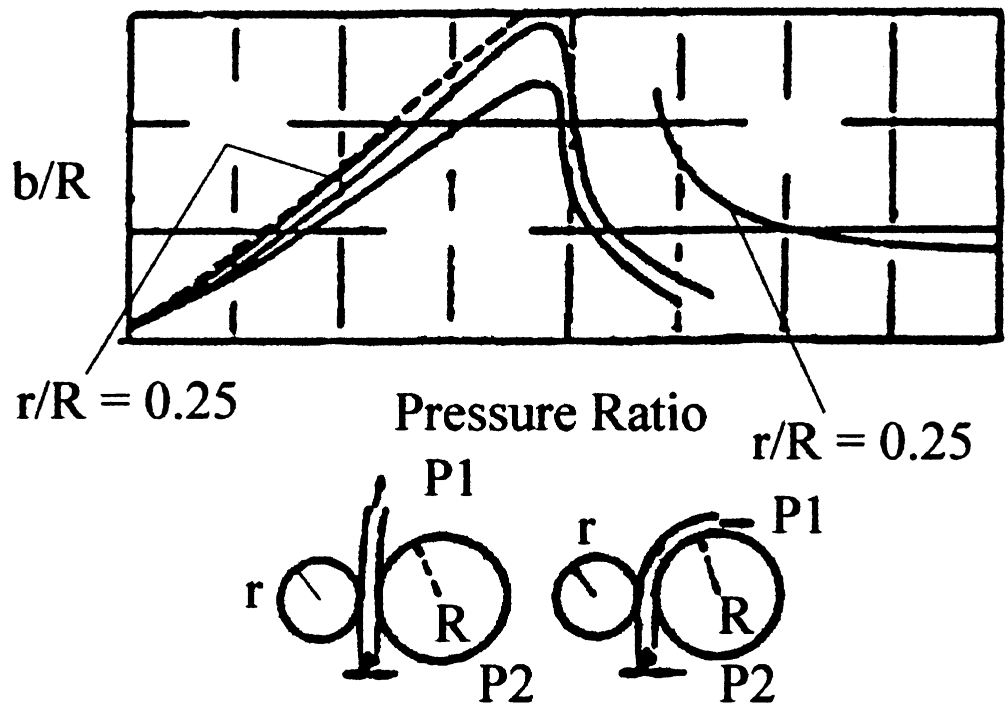

Figure 12: Relationship between b/R and r/R.
(Source:Fluid Induced Vibration of Steam Control Valves UDC 534.11.001.5:621.165-3)

3. Previous Research for a Three-Dimensional Test

The two-dimensional flow test has resulted in an understanding of a two-dimensional flow that concerns the free jet flow through the valve and valve seating. Adding in the third dimension, we now look at the one aspect omitted in the flow during the two-dimension test. This includes the random wake or a turbulent flow vortex, which will appear around the vicinity of the valve surface.

3.1 Three-Dimensional Model Test

The previous research test has shown us the relationship between the flow patterns and the static pressures and to observe the pressure variations on the valve surface as well as the valve seating. However, the flow in a real valve system is not two-dimensional and is in fact, axially right-left asymmetric three-dimensional.

Unlike the use of the Schlieren method to make the flow pattern visible in the two-dimensional flow, it is not possible to make the flow here visible at all, so the flow pattern has to be analytically determined using the results of the previous test. The main concerns for this analysis are: pressure variation, static pressure, temperature and valve acceleration in all directions on certain positions of the valve and valve seating. The 3-D experimental setup is more complicated than the 2-D setup. It basically consists of a plug-type valve and seating enclosed in a pressure-chest. Flow is directed through the inlet orifice and out through the seating. The lift is controlled via a simple lever. The main testing apparatus is shown below.

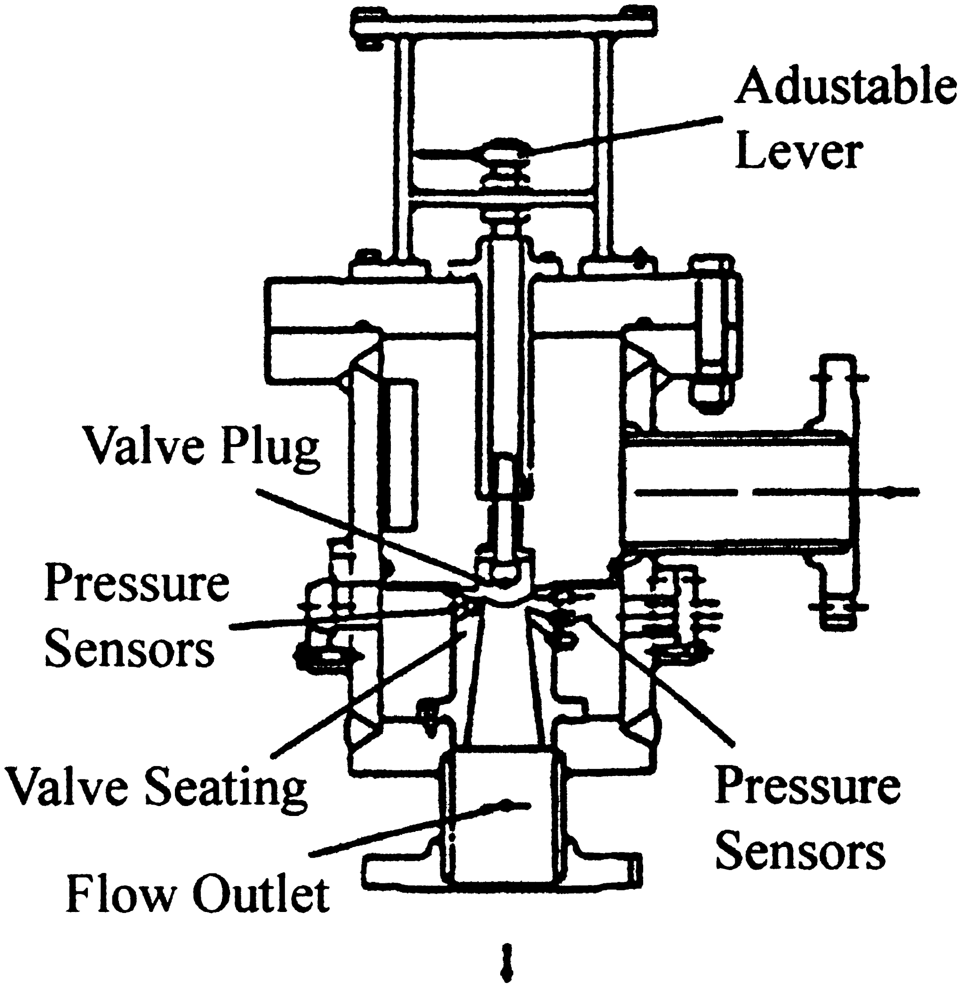

Figure 13: Main Testing Apparatus for Three-Dimensional Testing
(Source:Fluid Induced Vibration of Steam Control Valves UDC 534.11.001.5:621.165-3)

A 1/3 scale model was used, with natural frequencies in bending and longitudinal directions at about 300 Hz and 2500 Hz respectively. The actual valve frequencies vary as much as about 100 Hz and 700 Hz in the respective directions, but the testing was assumed that the scaling would compensate for this variation, and was concluded that the results can apply to reality. The source of flow was the same as used in the previous test, which was the main capacity tank and surge tank. Semiconductor pressure sensors were used and attached to positions between the throat and central portions of the valve at 90-degree intervals around the valve and one sensor in the center of the valve. Two sensors were attached to the valve seat, in the area of the wake flow and an accelerometer was also imbedded within the valve plug head. Figure 14 shows this arrangement.

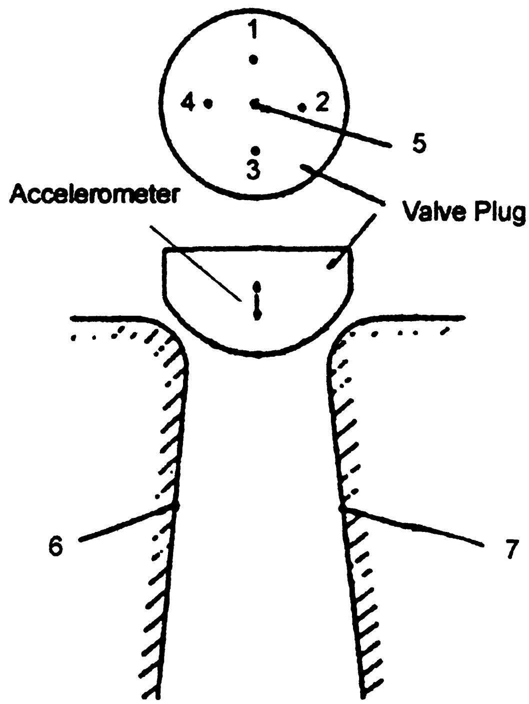

Figure 14: Positions of Pressure Sensors on Valve and Valve seating.
(Source:Fluid Induced Vibration of Steam Control Valves UDC 534.11.001.5:621.165-3)

The overall configuration, therefore, is shown above with four sensors positioned on the valve, two on the valve seating, and one accelerometer within the plug head.

3.2 Results and Observations of the Three-Dimensional Test

As mentioned, the flow pattern of the three dimensional test cannot be made visual, so its analysis must be correlated to the flow pattern observed in the two-dimensional test. The free jet flow is observed here, as well as the adherence to the valve surface during high pressure ratios. The vibration of flow at irregular intervals is also observed, but in the form of rectangular waves. Jet flowing in contact with the valve surface has a random-varying pressure, with larger variations found in those areas that when the flow is separated. The flow direction also fluctuates where the flow is supersonic, with pressure variations occurring at one frequency. Static pressures on the valve surface where flow is in contact is also found to be lower than pressures found where the flow is not in contact with the valve surface. Lastly, the ratio of static temperature found in the valve outlet to the inlet total temperature decreases as the pressure ratio decreases. This decrease is gradual with contact flow and rapid with non-contact flow.

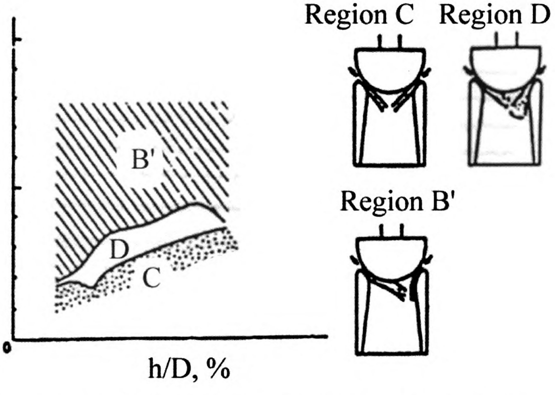

Figure 15: Flow Pattern of valve lift and pressure ratio for a Two-Dimensional Flow. (Source:Fluid Induced Vibration of Steam Control Valves UDC 534.11.001.5:621.165-3)

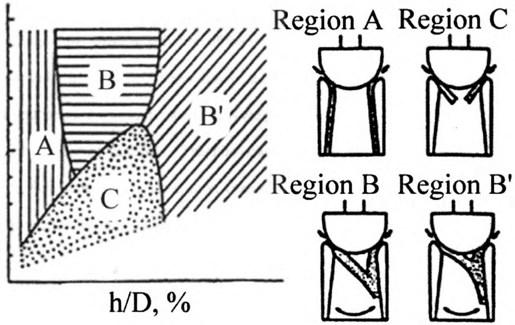

Figure 16: Flow Pattern of valve lift and pressure ratio for a Three-Dimensional Flow. (Source:Fluid Induced Vibration of Steam Control Valves UDC 534.11.001.5:621.165-3)

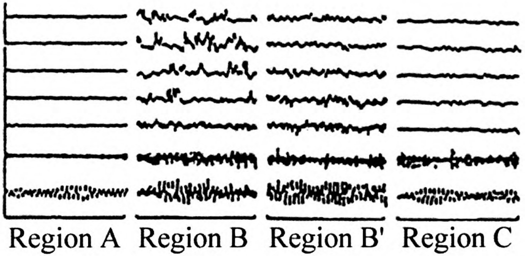

Figure 17: Time Traces of Valve Surface.
(Source:Fluid Induced Vibration of Steam Control Valves UDC 534.11.001.5:621.165-3)

The pressure variation waveform and the accelerator waveform at each point were also recorded with the imbedded accelerometer. The variations are large for when there is adhesion of flow to the valve surface, and the jet flow fluctuates. Changes in the flow pattern results in changes in the pressure waveform.

The magnitude of the pressure variation of the flow pattern (B) is large in the area of the throat and smaller in the center. Separation of the jet from the valve surface can also be observed, and is found where pressure pulses are produced at either the same time, or adjacently in 2 different directions. This phenomenon is also found in flow pattern (B'), but with the flow separation near the valve center.

This phenomenon is probably due to the random wake or turbulent flow vortex.

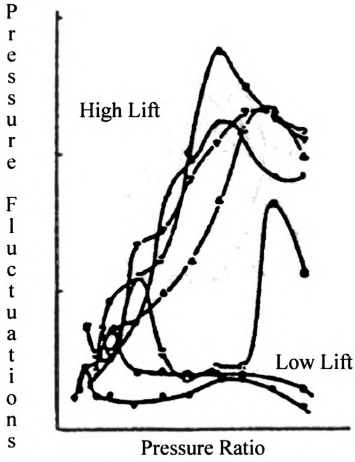

Figure 18: Surface Pressure Fluctuations.
(Source:Fluid Induced Vibration of Steam Control Valves UDC 534.11.001.5:621.165-3)

Figure 18 shows the data of amplitude of pressure variations as a relationship of pressure ratio and valve lift ratio, taken at the area of the valve throat. Figure 19 below shows the data of amplitude of pressure variations as a relationship of pressure ratio and valve lift ratio, taken at the area of the valve center.

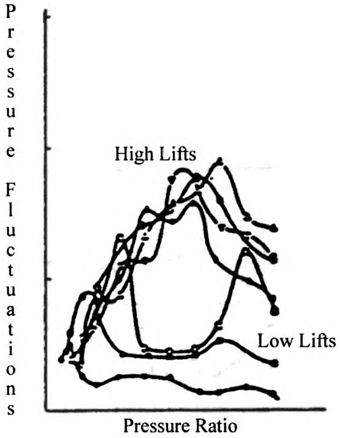

Figure 19: Surface Pressure Fluctuations.
(Source:Fluid Induced Vibration of Steam Control Valves UDC 534.11.001.5:621.165-3)

With a large valve opening, the pressure variation reaches a maximum at a ratio of 0.7, and with small valve openings, the same occurs at a pressure ratio of 0.2 to 0.3 and about 0.8.

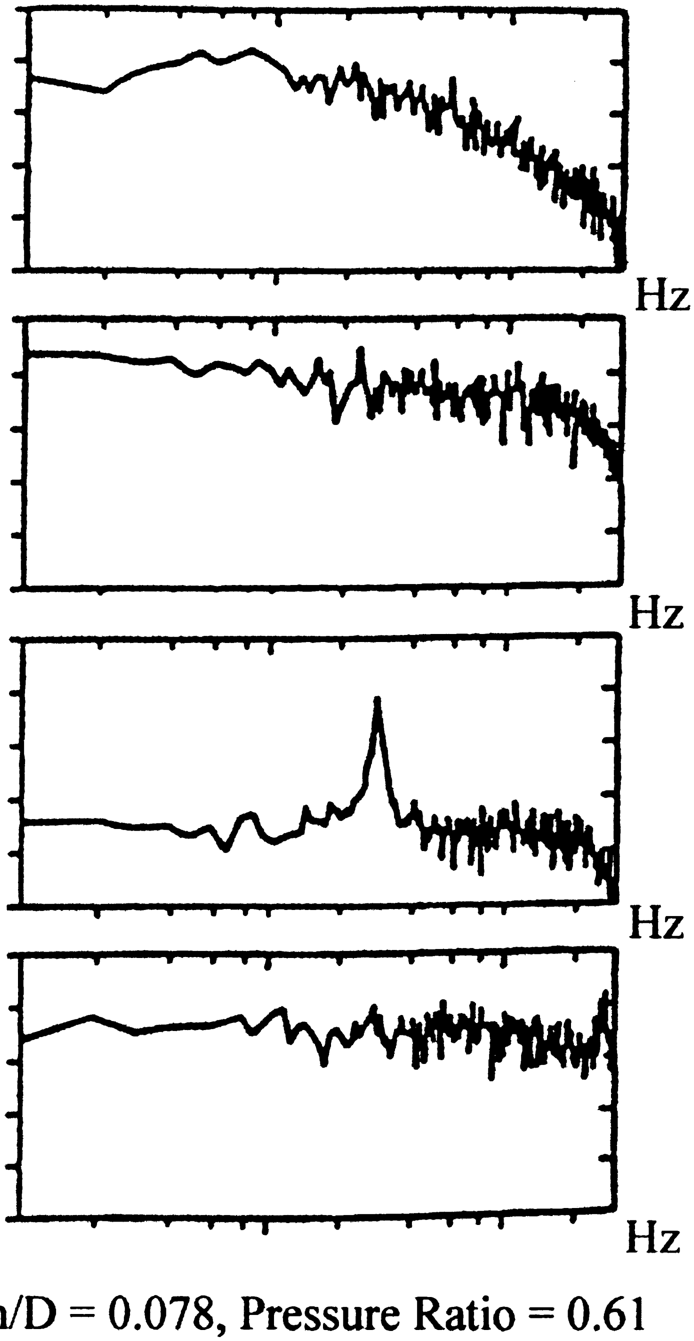

Figure 20: Power Spectra of Surface Pressure Fluctuation and Acceleration for the Three-Dimensional Model Valve. This spectra corresponds to the flow pattern (B) (Source:Fluid Induced Vibration of Steam Control Valves UDC 534.11.001.5:621.165-3)

It is shown that the pressure variation waveform can vary depending on the area in which the flow is analyzed. However, the vibration spectrum varies randomly without any outstanding features to the data as shown in figure 20.

As mentioned, the valve natural frequencies were 300 Hz and 2500 Hz in the lateral and longitudinal directions respectively. There are significant valve accelerations corresponding to these frequencies, resulting in a resonance type excitation caused by unsteady hydraulic forces. Accelerations were found to be extremely high in the region of great pressure ratios with large valve openings, and high in regions with small pressure ratios with small valve openings. This phenomenon was found in both the lateral and longitudinal directions.

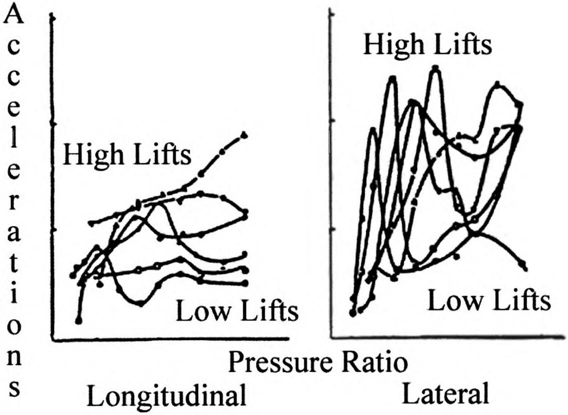

Figure 21: Vertical and Horizontal Accelerations for Model Valve as a relationship of pressure ratios for different valve lift ratios.
(Source:Fluid Induced Vibration of Steam Control Valves UDC 534.11.001.5:621.165-3)

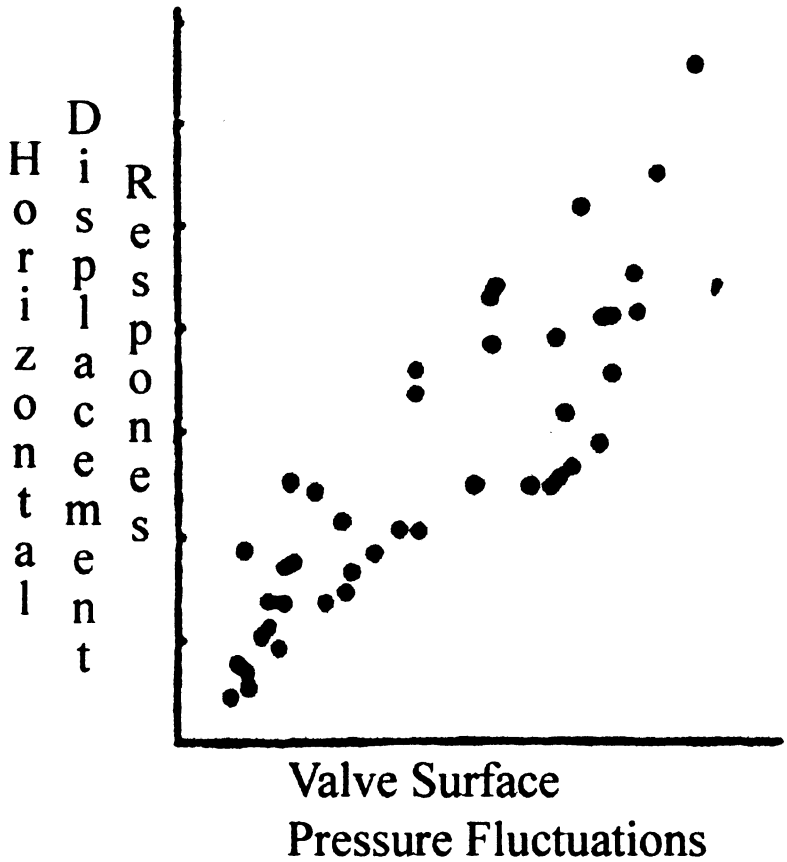

Figure 22: Horizontal Displacement Response against Valve Surface Pressure Fluctuation (Source:Fluid Induced Vibration of Steam Control Valves UDC 534.11.001.5:621.165-3)

The varying working force on the valve surface can be determined by integrating the pressure variations over the entire surface. Pressure variations occur when fluid flows or when a pressure wave is transmitted, resulting in a smaller integrated force result. However, this approximation is based on small pressure changes and no spatial correlation, so the result is slightly larger. The equation below calculates the Root Mean Square (RMS) value of the vibration amplitude. This is based on the assumption that the power spectrum density is flat in the area of the resonance point.

$$\sqrt{\overline{x^2}} = \sqrt{Wq(p)\frac{x}{4}\frac{p}{\varsigma}} \times A \qquad (3)$$

where Wq(p) is the power spectrum density, p = √(k/m), ζ= C/2pm, and p, ζ, and A are constant. There is a linear relationship between the square root of the power spectrum density of the fluid force and the RMS value of the vibration displacement, as shown in figure 22. Even though the plotting is scattered, it can be observed that there is a linear relationship between the two variables, and therefore equation (3) can be a used for a good approximation.

3.4 Application of the Model Testing to the Actual Valve System

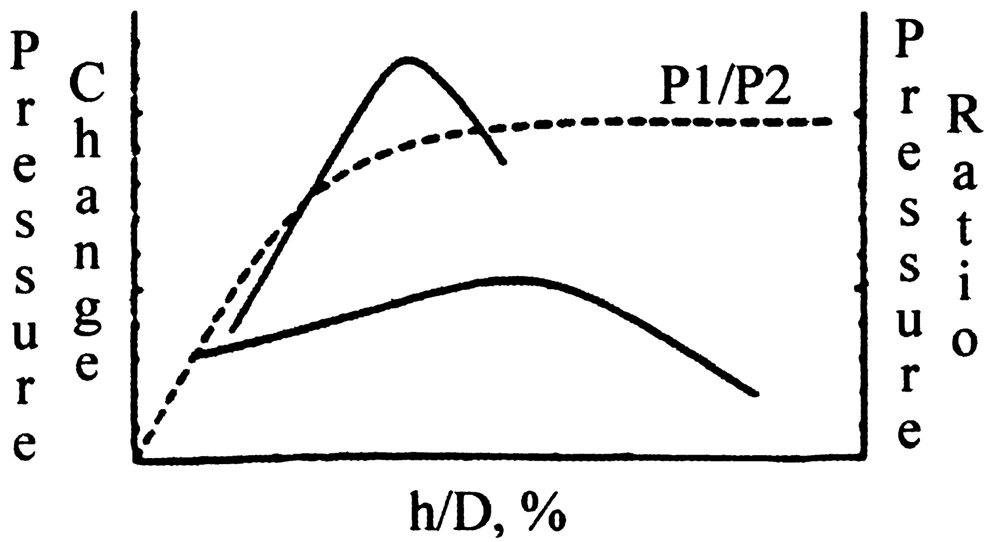

Figure 23: Typical valve Lift Characteristic Curve.
(Source:Fluid Induced Vibration of Steam Control Valves UDC 534.11.001.5:621.165-3)

The above figure describes the typical valve lift characteristic profile for a plug type valve. With an increase in the valve lift ratio, the pressure change between the valve inlet and outlet will increase, and the pressure ratio increases. With a ¼ valve lift, the pressure ratio is about 0.8. With a ½ lift, the pressure ratio becomes about 0.98. Looking back at figure 16, the region A signifies a small pressure variation, at a small valve lift ratio. As this ratio gets to about 0.05, the pressure ratio goes to 0.7 and enters region B, where the pressure variation starts to increase. Region B is also reached when the opening ratio is 0.15 with a pressure ratio of 0.98. Pressure variations will reach a maximum at a pressure ratio of 0.8, corresponding to regions B and B'. The pressure variation will decrease after the pressure ratio goes beyond that.

Based on these results, it can be concluded that the valve vibration is a result of non-steady flow, and that self-excited flow does not occur. The fluid force due to the valve vibration acts as a negative damper in the testing. The best method of reducing the vibration in the valve would be to redesign the valve and seating shapes so that fluid forces would not have that much of an effect on the valve to induce the vibration.

CHAPTER 4
Simple Theoretical Research of Self-Induced Vibration

1. Self-Induced Vibration

Self-induced vibration is the product of aerodynamic instability, and this field is growing largely into a very concerning aspect of turbine technology. As mentioned, valve inlet systems are very vital to the entire turbine system itself, with its failure to function bringing with it the entire malfunction of the turbine. This section will discuss the fundamentals of theoretical calculations for fluid-force estimation and stability of the valve. Doing so will provide a better comprehension to the results obtained through experiments and in comparing them to theoretical results, whether the data is valid and can be used for checking. It is meant to complement the experimental portion of the entire research, which is explained in chapter five.

2. Simple Theory of Self-Induced Vibration

This theory is usually complemented with a series of airflow tests that involve types of valves. During the tests, the self-excited vibrations of the plug were observed and was concluded that this occurred as a combination of aerodynamic forces on the valve plug surface and the vibrational characteristics of the plug structure. These tests were conducted based on the law of similarity for the fluid-flow induced vibrations. It is rather difficult to relate this, and there were some problems encountered, but the prediction of instability for the valve can be done with this use of the similarity law. With the measurement of aerodynamic forces and valve lift in testing, it was possible to predict the instability of the plug based on an eigenvalue analysis code.

2.1 Fluid Force Estimation

The fluid force estimation was based on plug model that assumed that the valve stem was rigid in the longitudinal direction, and that the lateral direction portion of the structural characteristic can be estimated with a spring-mass-damper system. This analysis only concentrates on the lateral vibration, or bending of the valve, and assumes that the longitudinal direction, or the direction of the stem, is a rigid body. This assumption can be made, because it is more likely that bending would occur at a much larger magnitude that longitudinal vibrations. However, in real testing, longitudinal vibrations must be included. The model for this analysis is shown below.

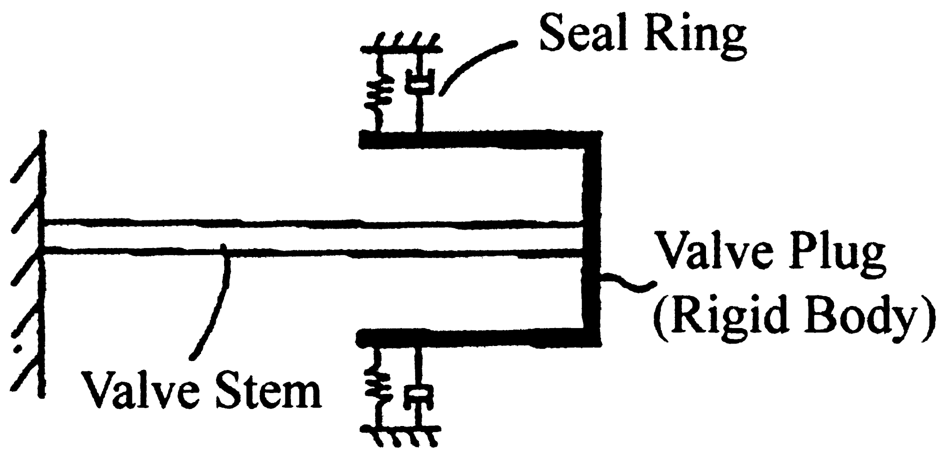

Figure 24: Theoretical Vibrational Model for Analysis
(Source: Study of Self-Excited Vibration of Governing Valves for Large Steam Turbines, Mitsubishi Heavy Industries, Ltd)

This analysis is based on small vibration amplitudes. The equation of motion for the model above is shown in a matrix form.

$$\begin{pmatrix} K_{xx} & K_{xy} \\ K_{yx} & K_{yy} \end{pmatrix}\begin{pmatrix} x \\ y \end{pmatrix}+\begin{pmatrix} C_{xx} & C_{xy} \\ C_{yx} & C_{yy} \end{pmatrix}\begin{pmatrix} \dot{x} \\ \dot{y} \end{pmatrix}+\begin{pmatrix} M_{xx} & M_{xy} \\ M_{yx} & M_{yy} \end{pmatrix}\begin{pmatrix} \ddot{x} \\ \ddot{y} \end{pmatrix}=\begin{pmatrix} F_x \\ F_y \end{pmatrix} \tag{4}$$

where,

k_{xx}, k_{xy}, k_{yx}, k_{yy} are from the sum of flows: induced stiffness and stem stiffness

C_{xx}, C_{xy}, C_{yx}, C_{yy} are from the sum of flows: induced damping and stem damping

M_{xx}, M_{xy}, M_{yx}, M_{yy} are the sum of the added masses and valve masses

F_x, F_y are the inducing forces

x, y are the valve displacements in the x and y axes

The above equation can be simplified to a simple matrix form, but with the matrix coefficients taking the form of equations.

$$\begin{pmatrix} Z_{xx} & Z_{xy} \\ Z_{yx} & Z_{yy} \end{pmatrix}\begin{pmatrix} x \\ y \end{pmatrix} = \begin{pmatrix} F_x \\ F_y \end{pmatrix} \tag{5}$$

where,

$Z_{xx} = K_{xx} + i\omega C_{xx} - \omega^2 M_{xx}$

$Z_{xy} = K_{xy} + i\omega C_{xy} - \omega^2 M_{xy}$

$Z_{yx} = K_{yx} + i\omega C_{yx} - \omega^2 M_{yx}$

$Z_{yy} = K_{yy} + i\omega C_{yy} - \omega^2 M_{yy}$

F_x and F_y are calculated from the output of the pulse counter targeted for the unbalanced mass, and the x and y displacements are measured by a displacement sensor. The unknown coefficients of the four Z values are determined using certain relationships to equation (2). The Z coefficients were determined using two forms of excitation, a forward circular excitation and a backward circular excitation.

The forward circular excitation matrix form

$$\begin{pmatrix} Z_{xx} & Z_{xy} \\ Z_{yx} & Z_{yy} \end{pmatrix} \begin{pmatrix} x_F \\ y_F \end{pmatrix} = \begin{pmatrix} F_{xF} \\ F_{yF} \end{pmatrix} \tag{6}$$

The backward circular excitation matrix form

$$\begin{pmatrix} Z_{xx} & Z_{xy} \\ Z_{yx} & Z_{yy} \end{pmatrix} \begin{pmatrix} x_B \\ y_B \end{pmatrix} = \begin{pmatrix} F_{xB} \\ F_{yB} \end{pmatrix} \tag{7}$$

The sum of the fluid forces coefficients and structural coefficients can be determined from the combination of the matrixes above to the following matrix form.

$$\begin{pmatrix} Z_{xx} \\ Z_{xy} \\ Z_{yx} \\ Z_{yy} \end{pmatrix} = \begin{pmatrix} x_F & y_F & 0 & 0 \\ 0 & 0 & x_F & y_F \\ x_B & y_B & 0 & 0 \\ 0 & 0 & x_B & y_B \end{pmatrix}^{-1} \begin{pmatrix} F_{xF} \\ F_{yF} \\ F_{xB} \\ F_{yB} \end{pmatrix} \tag{8}$$

All of the matrix equations above can easily be solved using simple matrix algebra and rules. The above equations would provide the results for the coefficients, which include the mass of the valve, the valve stem stiffness and the damping. The fluid forces are easily obtained by subtracting the coefficients with compliance without flow from the coefficients with compliance with flow. Thus, the fluid forces obtained would be a function of frequency. Figure 25 shows this relationship.

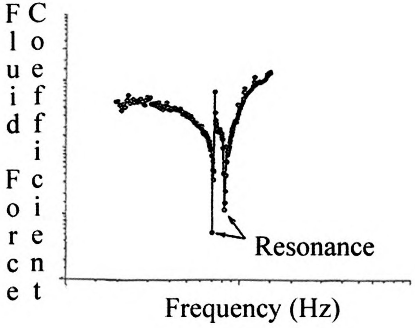

Figure 25: Relationship of Fluid Force Coefficient in Terms of Frequency
(Source: Study of Self-Excited Vibration of Governing Valves for Large Steam Turbines, Mitsubishi Heavy Industries, Ltd)

2.2 Stability

The stability analysis is conducted in conjunction with the fluid flow coefficients obtained from the equations above. The equation of motion for stability is show below:

$$\begin{pmatrix} M_{st} & 0 \\ 0 & M_{st} \end{pmatrix}\begin{pmatrix} \ddot{x} \\ \ddot{y} \end{pmatrix} + \begin{pmatrix} C_{st} & 0 \\ 0 & C_{st} \end{pmatrix}\begin{pmatrix} \dot{x} \\ \dot{y} \end{pmatrix} + \begin{pmatrix} K_{st} & 0 \\ 0 & K_{st} \end{pmatrix}\begin{pmatrix} x \\ y \end{pmatrix}$$
$$= \begin{pmatrix} \overline{M}_{xx} & \overline{M}_{xy} \\ \overline{M}_{yx} & \overline{M}_{yy} \end{pmatrix}\begin{pmatrix} \ddot{x} \\ \ddot{y} \end{pmatrix} + \begin{pmatrix} \overline{C}_{xx} & \overline{C}_{xy} \\ \overline{C}_{yx} & \overline{C}_{yy} \end{pmatrix}\begin{pmatrix} \dot{x} \\ \dot{y} \end{pmatrix} + \begin{pmatrix} \overline{K}_{xx} & \overline{K}_{xy} \\ \overline{K}_{yx} & \hat{K}_{yy} \end{pmatrix}\begin{pmatrix} x \\ y \end{pmatrix} \quad (9)$$

where,

$\overline{M}_{ij}$ is the added mass, $\overline{C}_{ij}$ is the induced damping, $\overline{K}_{ij}$ is the flow-induced stiffness,

M_{st} is the valve mass, C_{st} is the stem damping, and K_{st} is the stem stiffness

This equation can be made to the eigenvalue matrix form as shown below.

$$\left\{\lambda\begin{pmatrix} M & 0 \\ 0 & 1 \end{pmatrix}+\begin{pmatrix} C & K \\ -1 & 0 \end{pmatrix}\right\}\{X\}=0 \tag{10}$$

Instability occurs when the real part of the complex eigenvalues become positive. The matrix forms for M, C, and K depend on frequency, and they all add up to result in the fluid force coefficients and the structural coefficients. To find the frequencies that determine the M,C, and K coefficients, we assume a frequency and plot them against calculated damping ratios and calculated frequencies. The coefficients that are required are the ones that the imaginary parts of the eigenvalues agree. Examples of these 2 graphs are shown below.

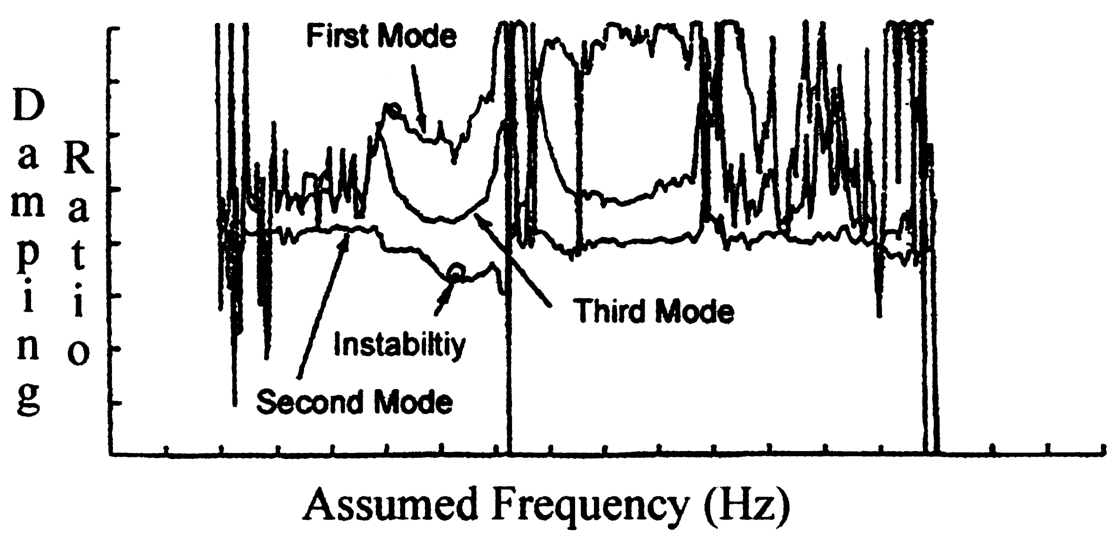

Figure 26: Relationship of Damping Ratio and Assumed Frequency
(Source: Study of Self-Excited Vibration of Governing Valves for Large Steam Turbines, Mitsubishi Heavy Industries, Ltd)

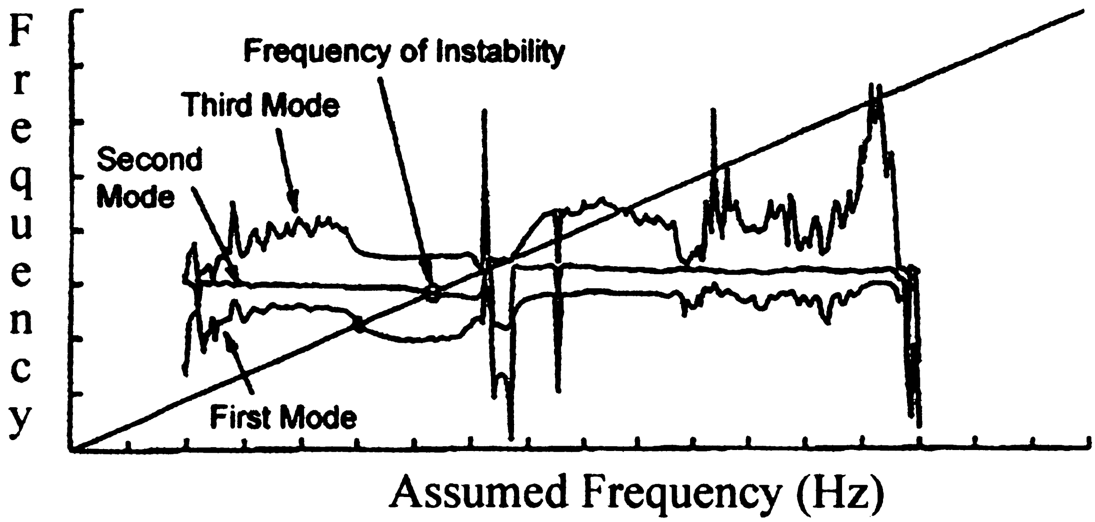

Figure 27: Relationship of Actual Frequency and Assumed Frequency
(Source: Study of Self-Excited Vibration of Governing Valves for Large Steam Turbines, Mitsubishi Heavy Industries, Ltd)

Looking at figure 26 and 27, we see three curves representing each of the three natural modes that occur from the relationship. In this case, by looking at the first mode curves in both figures, the first mode frequency and damping ratio is 50Hz, and 0.12. The second mode yields 65 Hz, and 0.04. Therefore, it is concluded that the first mode is stable, while the second mode isn't.

From this study, the frequencies, vibration modes and damping values can be determined from air-flow tests, much like the method examined in Chapter 3. These results can easily be extended to obtain an estimation of the performance of an actual machine by just looking at the structural and fluid properties. The predicted frequencies from the eigenvalue method are also accurate as compared to the experimental results as well. With these positive results, it is possible to estimate and predict behavior and self-excited forces on the valve structure without heavy use of experimental tests.

CHAPTER 5
The Current Research on the Quad-Valve System

1. General Problems Found from the History of Valve Failure Study

1.1 Instability Commencement of Valves

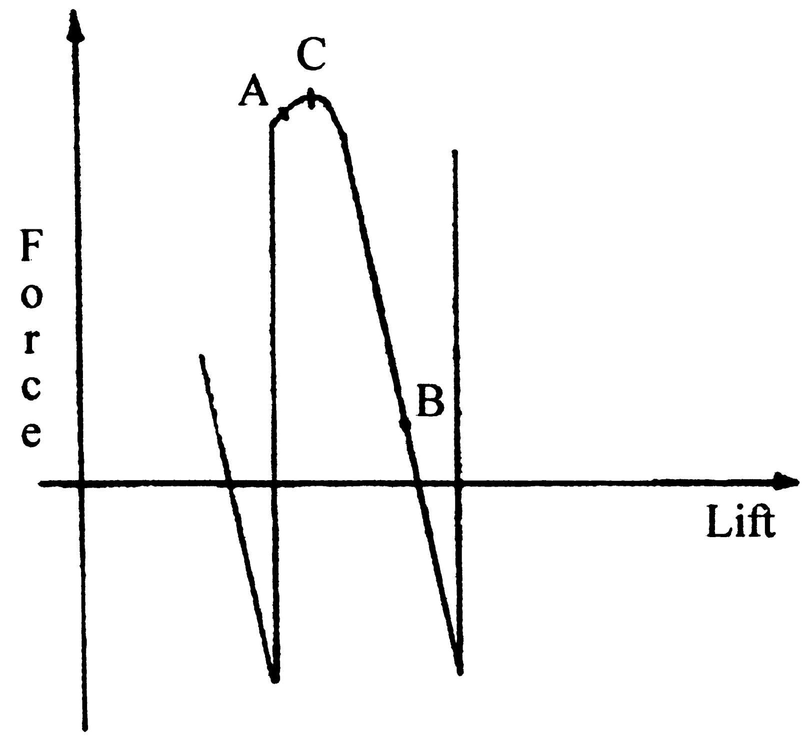

Figure 28: Relationship of Vertical Force on a Valve to the Valve Lift.
(Source Elliot Turbo-Machinery Co., 1976)

This figure shows the typical cycle and force experienced on a valve. It has been concluded in the past that anytime there is a negative slope present in a force-lift graph, there will be instability. The instability is dependent on the equivalent spring stiffness, the damping and the value of the negative slope of this relationship. Point A on the graph represents the force due to a partial loading on the turbine. The loading is then changed to correspond to point B on the graph. Point A is considered stable because it is during a positive slope and the servo-system operates in an "open valve" mode so it provides force to sustain the lifting force at point A. Point B, however, is unstable because it is along a negative slope. This slope corresponds to the change in opening from point A to B, but requires the servo-system to supply additional force to go from point A to point C. But after the point C, the force on the valves drops while the servo-system is supplying an even higher force than C within the response time. This means that depending on the system damping, the negative force slope, and the servo-force characteristics, the valves will open in an accelerated rate to point B and continue to open till it reaches the next valve and tries to open it. During that time, the turbine speed will increase and the turbine governors will signal the servo-systems to close the valves because the steam flow is larger than necessary for the turbine loading. If the steam flow does not meet the turbine loading needs, the turbine will signal the servo-system to open the valves again, and the cycle repeats itself. It is believed that the description of the above phenomenon is the start of a valve vibration problem that tends to lead to a more fatigue type problem, which is the cause of this valve failure.

The turbine speed will increase and the turbine governors will signal the servo-systems to close the valves because the steam flow is larger than necessary for the turbine loading. If the steam flow does not meet the turbine loading needs, the turbine will signal the servo-system to open the valves again, and the cycle repeats itself. It is believed that this phenomenon is the start of a fatigue type valve failure.

1.2 Bending Loadings

Other valve forces that tend to lead to the fatigue problem of valve failure come from bending loadings. From the potential flow theory, if the sink flow rate is uniform, there will be a force on the sink.

$$F = \frac{\dot{m}U_0}{g_0} \tag{11}$$

where F is the force on the sink, $\dot{m}$ is the sink flow rate, U_0 is the uniform flow, and g_0 is the gravitational constant.

If we represent the valve as such with a sink in uniform flow of velocity equal to the steam velocity in the steam chest, the force F will cause a bending moment, with a bending stress calculated with the equation below

$$\sigma_b = \frac{32M_b}{\pi d^3} = \frac{32}{\pi}\left(\frac{FL}{d^3}\right) = \frac{32}{\pi}\frac{\dot{m}UL}{g_0 d^3} \tag{12}$$

where $\dot{m}$ is the mass flow rate, U is the steam velocity at the steam chest, d is the stem diameter, L is the stem length, and g_0 is the gravitational constant.

1.3 Valve Spinning

As the phenomenon indicates, this occurs when some form of torque is present on the valve, which will cause spinning of the valve if it is not somehow rigidly positioned. The only cause of this valve spinning is the fluid and how it flows. The torque is induced by a change in angular momentum as it passes through the valve. This can occur from many reasons, but the two most common reasons are as follows:

1) Non-uniform velocity distribution at the steam chest
2) Eccentricity between the valve and its seating

If the potential flow model of a sink is considered again, but in a parallel flow, it is observed that due to the non-uniformity of the external flow, U, the separating streamline will be unsymmetrical. This causes a resultant force, and hence, a resultant torque caused by the force acting perpendicular on a moment arm that starts from the sink to the point of action of the force. This also causes an additional effect, which is the second of the two reasons mentioned above.

Valve eccentricity is more easily comprehensible at a 2 dimensional view.

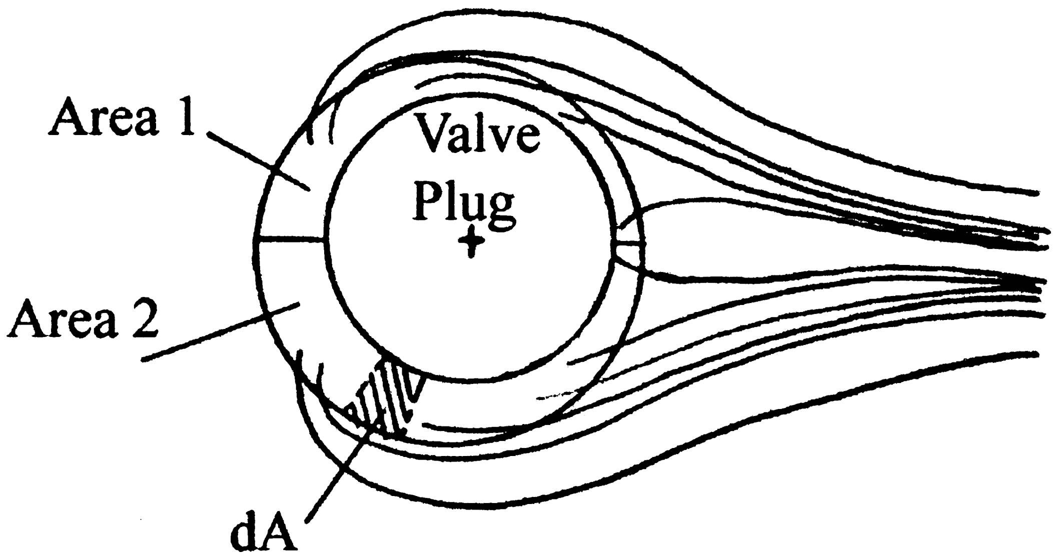

Figure 29: Two-Dimensional View of Plug Eccentricity

The mass flow rate through the valve is given by the equation

$$d\dot{m} = \rho U dA \tag{13}$$

where U is perpendicular to dA. From this, the total mass flow rate is given by

$$\dot{m} = \int_0^{2\pi} d\dot{m} = \int_0^{\pi} d\dot{m} + \int_{\pi}^{2\pi} d\dot{m} \tag{14}$$

With the assumption that the flow area at this point is minimum with a choked flow, thus making the density and the velocity constant, we have the mass flow rate as:

$$\dot{m} = \rho U \left[\int_0^{\pi} dA + \int_{\pi}^{2\pi} dA \right] = \rho U (A_1 + A_2) \tag{15}$$

Angular momentum change of the fluid is given by

$$dM_{ang} = \frac{D}{2} V d\dot{m} \tag{16}$$

where V is the tangential velocity component to the plug surface and D is the valve plug diameter.

Therefore, the net change in angular momentum can be found with the general equation.

$$\Delta M_{net} = \int_0^{2\pi} \frac{D}{2} V d\dot{m} = \int_0^{\pi} \frac{\rho U D}{2} V dA - \int_0^{-\pi} \frac{\rho U D}{2} F dA$$

$$= \frac{\rho U D}{2} \left[\int_0^{\pi} V dA - \int_0^{-\pi} V dA \right] \tag{17}$$

This equation can be simplified for some special cases. One special case is if it was assumed that the tangential velocity component is symmetrical around the valve plug, the equation becomes

$$\Delta M_{net} = \frac{\rho U D}{2} \int_0^{\pi} V (dA_1 - dA_2) \tag{18}$$

Another special case, which is the assumption that there is no change in angular momentum, the equation simplifies to

$$\int_0^{\pi} V dA = \int_0^{-\pi} V dA \tag{19}$$

This can be further simplified to Vav1A1 = Vav2A2 and since the areas and the velocities terms are not equal, the boundary layer will thus not be symmetrical around the valve plug surface. Accordingly, a frictional force will cause the torque to the valve stem. Therefore, with these 2 assumptions, a resultant torque will always be present.

2.Research Problem with Quad-Valve System

From the previous sections describing the previous research on this problem, and previous subsequent testing, data acquired from past research has shown insufficient data to really determine the basic mechanism that causes the valve vibration and subsequent failure. However, simple forced response has been speculated to not be the problem. With the size and type of the valve system in study, with a high mass flow rate; it would seem to suggest that there is a high probability that the root cause of the valve vibration is caused by an instability mechanism. Increases in steam chest pressures and the resulting mass flow rate are the causes of this instability. It is also thought that the changes in stem stiffness with the resulting change in valve lateral resonant frequencies are also contributing factors. With the presence of large dynamic pressures upstream and downstream, it is still unclear whether these pressures contribute to the strong lateral response. The best solution for investigating the vibrations in the quad-valve system would be to use a reduced or full-scale modeling and testing method. The possibility of unsteady fluid forces generated from the transition from choked to unchoked flow, as the lift increases, has not been completely omitted from the analysis as the causes of the valve vibration and failure. Depending on the results of the testing, if the cause of the vibration is not from instability but from unsteady fluid forces from the pressure field around the valve, the tests should still be able to record any data that would assist in documenting the dynamic loadings.

2.1 Preliminary Theoretical Calculations of Valve Flow

During operation when inducted with the steam turbine, the 2nd and 3rd valve seem to break the most often under operation, with the 2nd valve being the primary breakage valve, and at various times. Below is a picture of the four-valve system under study.

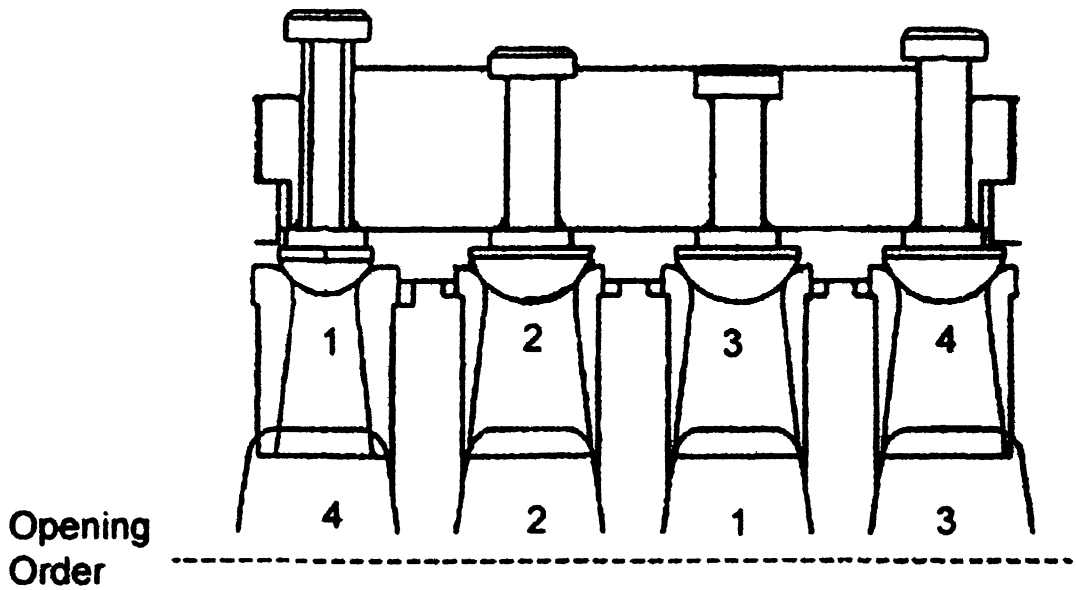

Figure 30: Four-Valve System.

Many experimental designs were brainstormed, most with singular or dual valve systems. The actual valve design is of a regular plug-type valve. The actual shaft, however, has been altered to a square shaft with chamfered corners. The shaft has been redesigned from a pure circular cross section to this chamfered square shaft cross section to eliminate the presence of change in angular momentum caused by non-uniform velocity distribution or valve eccentricity, which causes valve spinning, as mentioned in the previous section. The valve opening sequence is the 3rd valve, then the 2nd, with the 4th valve after that, and the 1st valve to finish the sequence. Flow charts of various valve lifts, were also charted, with problems or observed theoretical instability occurring at lifts of 0.454 and 0.639 inches. The instability is most notable when the lift is at 0.639 inches.

The experimental rig design was finally confirmed with a singular valve design. The valve stem was kept circular but a locking mechanism will be used to ensure fixed positioning of the valve during operation. The valve chest initially had a strong transparent window on one of the sides of the valve chest for outside observation, but was eventually dropped for simplicity and the fact that it is impossible to physically observe the flow. The range of pressure ratio is from 1 to 3 and the flow through the valve at each pressure increment was calculated at choked flow to find the maximum flow properties. This theoretically will be the result that can be used for comparison with the actual test data obtained. With a high flow rate obtained in the calculations with a full-scale sized valve, a size reduction was made to ½. At this scale, the size of the valve would just be adequate to accommodate all the static and dynamic pressure gauges required to obtain the necessary data. Even at ½ scale, the flow rate is still high, and the use of a compressor or large blower could prove hazardous at such high flow rates. Therefore, the alternative, which is to use some sort of vacuum device to suck the flow through the chest, would be less hazardous and perhaps provide a more simplified testing method.

3. Preliminary Design concepts and Calculations to Scaling

Based upon the actual pressure chest design and previous research done on similar problems from various turbines, accurate information can be obtained from a single valve design at a relatively small scale. It was, however, desired that the scale be as large as possible with possibly a full quad-valve design to observe the total behavior of the actual valve design. After much consideration to the easiest path to observing the valve behavior, the first reduction to the test design was to a dual valve design at full scale. A simple concept of this is shown below.

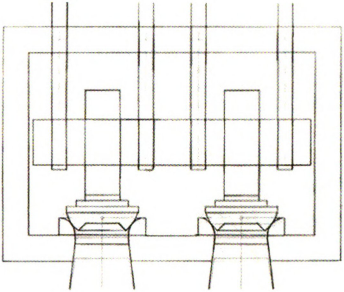

Figure 31: Early Dual-Valve

After further discussions with the people from Elliot Turbo machinery Company, a singular valve design was adequate for the analysis, even though that perhaps the analysis of two valve operating together would be vital in the influence of the valves on one another during operation. This however, was not nearly as important as decreasing the time and cost to construct the valve when a singular valve design would still be adequate in analyzing the valve behavior, since the 2nd valve was the primary breakdown valve.

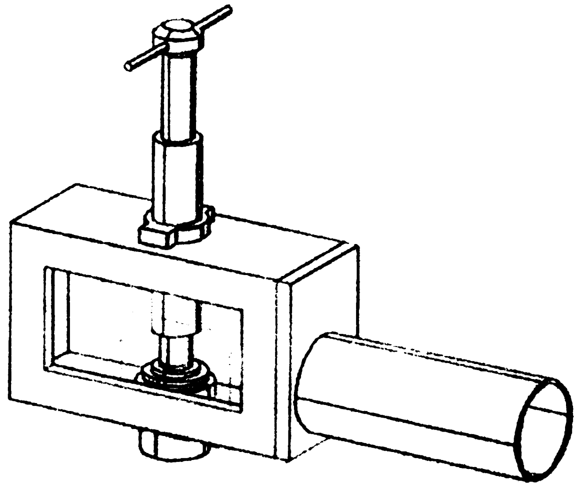

Figure 32: Early concept of Singular Valve Design

Several calculations had to be made to theoretically observe the flow rate through the design and then the search for the appropriate vacuum pump that can provide such a flow can be researched and found.

3.1 Method of Flow Calculations

This is done with several important initial conditions, using some equations that relate to thermodynamics of high-speed fluid flow.

Conditions	Units
Ratio of specific heats of the fluid (k)	Dimensionless
Specific heat at the inlet static temperature (C_p)	J/kg-K (Btu/(slug-°R)
Gas constant for the fluid (R)	Pa-m^3/kg-K (ft-lbf/slug-°R)
Venturi Area (A_v)	m^2 (ft^2)
Static inlet temperatures (T)	K (°R)
Stagnation inlet temperatures (T_0)	K (°R)
Static inlet pressures (P)	bar or Pa (lbf/ft^2)
Stagnation inlet pressures (P_0)	bar or Pa (lbf/ft^2)
Mass flow rate ($\dot{m}$)	kg/s (slug/s)
Flow rate at the inlet (v)	m^3/s (cfm)

Table 2. Properties for the Commencement of Flow Calculations

The calculation for density will be important for the determination of the mass flow rates. The formula that will be important here is of the form:

$$\rho = \frac{P}{RT} \tag{20}$$

where P is the pressure (static or stagnation), R is the Gas constant, and T is the temperature (static or stagnation). The idea of this initial calculation is to treat the flow as though it is going through a simple converging diverging nozzle.

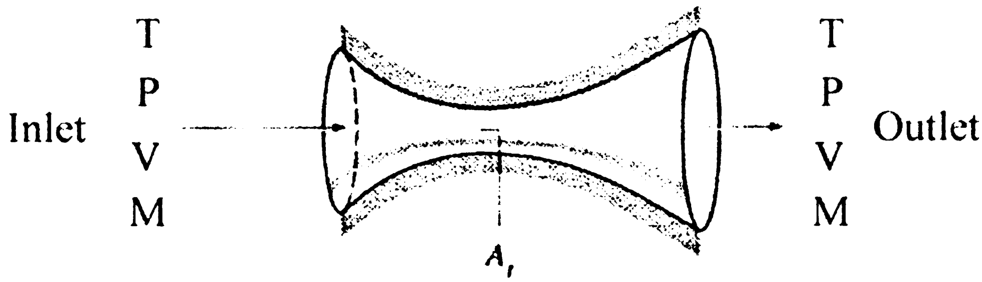

Figure 33: Simple Converging Diverging Theory

M	M*	A/A*	P/P_0	ρ/ρ_0	T/T_0
0	0	∞	1.00000	1.00000	1.00000
0.10	0.10943	5.8218	0.99303	0.99502	0.99800
0.20	0.21822	2.9635	0.97250	0.98027	0.99206
0.30	0.32572	2.0351	0.93947	0.95638	0.98232
0.40	0.43133	1.5901	0.89562	0.92428	0.96899
0.50	0.53452	1.3398	0.84302	0.88517	0.94238
0.60	0.63480	1.1882	0.78400	0.84045	0.93284
0.70	0.73179	1.09437	0.72092	0.79158	0.91075
0.80	0.82514	1.03823	0.65602	0.74000	0.88652
0.90	0.91460	1.00886	0.59126	0.68704	0.86058
1.00	1.00000	1.00000	0.52828	0.63394	0.83333
1.10	1.08124	1.00793	0.46835	0.58169	0.80515
1.20	1.1583	1.03044	0.41238	0.53114	0.77640
1.30	1.2311	1.06631	0.36092	0.48291	0.74738
1.40	1.2999	1.1149	0.31424	0.43742	0.71839
1.50	1.3646	1.1762	0.27240	0.39498	0.68965
1.60	1.4254	1.2502	0.23527	0.35573	0.66138
1.70	1.4825	1.3376	0.20259	0.31969	0.63372
1.80	1.5360	1.4390	0.17404	0.28682	0.60680
1.90	1.5861	1.5552	1.4924	0.25699	0.58072
2.00	1.6330	1.6875	0.12780	0.23005	0.55556

Table 3. The results of one-dimensional isentropic compressible-flow functions for an ideal gas with constant specific heats and molecular weights.

With the use of the table above, results can be easily found at the throat. This table records the results of one-dimensional isentropic compressible-flow functions for an ideal gas with constant specific heats and molecular weights.

However, the manual process can be done with three specific functions, each one relating to pressures, densities and temperatures.

$$\frac{P}{P_0} = \left(1 + \frac{k-1}{2} M^2\right)^{-k/(k-1)} \tag{21}$$

$$\frac{\rho}{\rho_0} = \left(1 + \frac{k-1}{2} M^2\right)^{-1/(k-1)} \tag{22}$$

$$\frac{T}{T_0} = \left(1 + \frac{k-1}{2} M^2\right)^{-1} \tag{23}$$

where P is the pressure, T is the temperature, M is the Mach number, and k is the ratio of specific heats. The velocity of the flow is used to calculate the resultant flow rates and mass flow rates. The equation used is:

$$v = \sqrt{kRT} \tag{24}$$

3.1.1 Initial Flow Calculations

These calculations are based on a ½ scale modeling of the actual valve system. The first method of calculation assumes that the Mach number reaches one at the throat, or that the flow becomes choked. The highest flow rate that would be experienced during the experiment is when the pressure is at a 3 to 1 ratio. This model also assumes that the flow rate maintains a Mach number of 1 through the throat and into the venturi area. The ideal gas is air, and the process is considered isentropic. There is also the introduction of a taft cut-off percentage of venturi flow area, which determines the minimum flow that maintains the pressure ratio, which is explained later. The initial conditions to commence these calculations are tabulated below.

Conditions	Units
Ratio of specific heats of the fluid (k)	1.4
Gas constant for the fluid (R)	287 (1714.4) Pa-m^3/kg-K (ft-lbf/slug-°R)
Venturi area (A_v)	0.001188 (0.012788) m^2 (ft^2)
Static inlet temperatures (T)	300 (540) K (°R)
Stagnation inlet temperatures (T_0)	300 (540) K (°R)
Static inlet pressures (P)	1 or 100000 Pa (2116.8) bar or Pa (lbf/ft^2)
Stagnation inlet pressures (P_0)	1 or 100000 Pa (2116.8) bar or Pa (lbf/ft^2)
Mass flow rate ($\dot{m}$)	0 kg/s (slug/s)
Flow rate at the inlet (v)	0 m^3/s (cfm)

Table 4. Initial Conditions

Using equation (20), we can determine both the static and stagnation densities. Since the inlet flow is negligible, the static and stagnation temperatures, pressures and the densities are all the same. Thus the density calculated is 1.16144 (0.002287) kg/m^3 or slugs/ft^3. Using table 3 or the equations (21) through (23), the temperatures, pressures and densities at the throat at choked conditions can be found. The temperature, pressure and density are found to be 250 (450) K (°R), 0.5354 bar or 53542 (1118.263) Pa (lbf/ft^2) and 0.748 (0.00145) kg/m^3 or slugs/ft^3. The resulting velocity through the throat using equation (24) is 316.88 (1039.63046) m/s (ft/s).

The more important results stem from the calculations in the venturi area, which is the main area of interest. As mentioned, the greatest flow occurs at a pressure ratio 3 to 1. With a vacuum pump, a pressure ratio of 3 to 1 would occur at a venturi pressure of 0.333333 bars if the inlet pressure were at 1 bar. Thus the pressure and density are just 1/3 of their values at the inlet. This makes them 0.3333 bar or 33333 (705.6) Pa (lbf/ft^2) and 0.392971 (0.000762171) kg/m^3 or slugs/ft^3.

The choked venturi mass flow rate is calculated using the equation:

$$\dot{m} = \rho V A \tag{25}$$

thus, obtaining a 0.28125 (0.019264) kg/s (slugs/s) mass flow rate, with the density and velocity results taken from the throat or choked position. The volumetric flow rate is simply the mass flow rate divided by the density, giving a 0.37633 (13.29) m^3/s (ft^3/s) flow rate. The volumetric flow rate at the venturi area, which will determine the flow that is required to simulate the operating conditions of the actual valve chest, is found to be 0.7157 (25.27471) m^3/s (ft^3/s), or 42.942 (1516.5) m^3/min (cfm) by dividing the choked mass flow rate with the density found at the venturi area. This flow rate is the desired flow rate in which to maintain a 3 to 1 pressure ratio at a wide-open valve lift of 0.639 inches. To find the minimum flow required to maintain this pressure ratio, the earlier mentioned taft cut-off percentage of venturi valve flow area is applied to the calculation. At a 0.016231 (0.639) m (inch) lift, the cutout position where instability was observed, the original valve (at full scale) had a flow area of 0.002793 (4.329) m^2 (in^2), which is 58.77% of the full-open venturi area. This percentage is the taft cut-off percentage of venturi valve flow area. Applying this to the 42.942 (1516.5) m^3/min (cfm) flow rate, the minimum flow rate to maintain the 3 to 1 ratio is found to be 25.237 (891.2367) m^3/min (cfm).

3.1.2 Secondary Flow Calculations

These calculations are basically similar to the to the ones for the initial calculations, but it is somewhat more accurate. The equations used are identical and the starting initial conditions are the same as in table 4. However, the calculations from the throat area to the venturi are not as simple as the factoring of the pressure ratio of 3 to 1 as in the previous calculations. With the same inlet conditions as shown in table 4, and with the use of equation (20), the static and stagnation densities are the same as before at the inlet conditions. Using table 3 or the equations (21) through (24), the temperatures, pressures and densities at the throat at choked conditions are 250 (450) K (°R), 0.52828 bar or 52828 (1103.336) Pa (lbf/ft^2) and 0.736283 (0.0014286) kg/m^3 or slugs/ft^3. The resulting velocity is 316.938 (1039.823) m/s (ft/s).

The venturi area is calculated in a similar fashion as from the inlet to throat position, than just the simple factoring of the pressure ratio, which was done in the previous calculations. With the known pressure ratio of 3 to 1, we use the table 3 or the equations (21) through (24) again to find the temperatures, pressures, and densities, which are 219.8655 (395.76) K (°R), 0.33333 bar or 33333 (705.6) Pa (lbf/ft^2) and 0.534453 (0.001037) kg/m^3 or slugs/ft^3. Using equation (24) the velocity through and out the venturi area is 401.252 (1316.4436) m/s (ft/s). The mass flow rate with equation (25) is 0.25477 (0.01746) kg/s (slugs/s). This gives us a volumetric flow rate of 0.47669 (16.834) m^3/s (ft^3/s) or 28.6014 (1010) m^3/min (cfm).

From the initial calculations, the flow rate calculated was 42.942 (1516.5) m^3/min (cfm), with a minimum flow rate of 25.237 (891.2367) m^3/min (cfm) to maintain the pressure ratio at 0.016231 (0.639) m (inch) lift. A more accurate calculation for the flow was 28.6014 (1010) m^3/min (cfm). The initial results were used for the selection of the flow system, as it would be trivial to use the higher flow rate to enable calculations and predictions on a possible worst-case scenario.

Throat position	Total Temp. K (R)	Static Temp. K (R)	Total Press. bar (lbf/ft^2)	Static Press. bar (lbf/ft^2)	Density Kg/m^3 ($slugs/ft^3$)	Velocity m/s (ft/s)	Mass Flow Rate kg/s (slugs/s)	Flow Rate m^3/s (ft^3/s)
Initial	300 (540)	250 (450)	1 (2116.8)	0.5354 (1118.3)	0.748 (0.00145)	316.88 (1039.63)	-	-
Secondary	300 (540)	250 (450)	1 (2116.8)	0.52828 (1103.34)	0.7363 (0.001429)	316.94 (1039.82)	-	-

Table 5. Results for Throat Position Calculations at Pressure Ratio of 3

Venturi position	Total Temp. K (R)	Static Temp. K (R)	Total Press. bar (lbf/ft^2)	Static Press. bar (lbf/ft^2)	Density Kg/m^3 ($slugs/ft^3$)	Velocity m/s (ft/s)	Mass Flow Rate kg/s (slugs/s)	Flow Rate m^3/s (ft^3/s)
Initial	300 (540)	250 (450)	1 (2116.8)	0.3333 (705.6)	0.748 (0.00145)	602.44 (1976.5)	0.28125 (0.01926)	0.7157 (25.275)
Secondary	300 (540)	219.866 (395.76)	1 (2116.8)	0.3333 (705.6)	0.534453 (0.001037)	401.252 (1316.4436)	0.25477 (0.01746)	0.47669 (16.834)

Table 6. Table of Results for Venturi Position Calculations at Pressure Ratio of 3

4. Scaling and Design of Experimental Setup

From the results above, the flow rates are exceptionally high, even with the half-scaling. It was, however, previously stated that the half-scale size was the bare minimum in terms of valve size to be able to fit the desired number of pressure gauges, both dynamic and static.

4.1 The Valve and Valve Chest

The final valve and valve chest design was made to be a single valve design, much similar to the concept drawing from figure 32. The single valve will replicate a simple plug-type valve used in the actual turbine machine. However, with the advent of pressure gauges on the valve and seating, room must be made for the wiring and simple access to them. The seating would not have much problem positioning the gauges and the wiring can easily be done to not interfere with the operation of the experimental setup. The valve, however, does prove some challenges in positioning the gauges as well as the wiring. The basic setup would have 3-4 rows of pressure gauges on the valve and 4-5 rows on the seating. Each row would have dynamic pressure gauges at the north-south-east-west positions, with 2 static pressure gauges at 45 degrees between 2 dynamic gauges at opposite ends. The configurations as well as the actual model valve dimensions are shown in Appendix B. The emphasis was on the dynamic pressures, since they are responsible for the stresses and vibrational forces experienced when the valve is under operation. Another consideration was that the pressure gauges on the valve plug and seating must be placed such that they are as close as possible to the surface as possible. At high flow rates, the slightest deformation on a surface could alter pressures at that area, altering the results in vibration amplitudes and stresses. The plug head itself can separate into 3 different pieces, the plug head, a mounting plate between the plug head and the stem, and the stem piece. The plug head and the valve stem will be made hollow to make way for the internal wiring of the pressure gauges. Four screws are used to attach all three pieces together. With Aluminum 2024 as the working material, it must be noted that preliminary calculations must be made for forces and stresses on the model valve to ensure that failure does not occur during the operation. From the information of Aluminum 2024 found in Appendix C, the yield stress of aluminum is 58000 psi. From chapter 5, section 1.2, which describes the potential theory of bending loadings, the equation for force on the sink is

$$F = \frac{\dot{m} U_0}{g_0} \tag{8}$$

where F is the force on the sink, $\dot{m}$ is the sink flow rate, U_0 is the uniform flow, and g_0 is the gravitational constant.

If we represent the valve as such a sink in uniform flow of velocity equal to the steam velocity in the steam chest, the force F will cause a bending moment, with a bending stress calculated with the equation below

$$\sigma_b = \frac{32M_b}{\pi d^3} = \frac{32}{\pi}\left(\frac{FL}{d^3}\right) = \frac{32}{\pi}\frac{\dot{m}UL}{g_0 d^3} \tag{9}$$

where $\dot{m}$ is the mass flow rate, U is the steam velocity at the steam chest, d is the stem diameter, L is the stem length, and g_0 is the gravitational constant. Using the initial calculation values for the theoretical flow through the testing setup, the total force on the sink is about 20.01 lbf. The resulting axial stress is 51090 psi. This number is less than the aluminum yield stress, so the valve will hold up during operation.

Valve lift control is made from using an internally threaded shaft. The main valve stem will be externally threaded and will go through the shaft. A simple lever mechanism is attached to the top of the stem once through the shaft. The valve lift is set by screwing the stem to the proper position and then immobilized with 2 simple lock nuts, one on each end of the shaft. This entire mechanism is attached to the valve pressure chest. The pressure chest is made large enough such that the flow and the initial conditions of pressure, temperature, density, and flow velocity does not change as the flow reaches through the passageway created by the valve. The dimensions to the current development of the pressure chest are shown in Appendix B. To simulate as close as possible the flow into the pressure chest, the inlet orifice is exactly ½ scale to the actual orifice size. The exit orifice is the same size as the valve seating component.

4.2 The Flow System

With the scale of the experimental setup limited to the pressure gauge configuration, the next step was to select a method of producing the flow through the setup. The higher flow from the initial theoretical calculation was selected to plan the setup, to assure that any discrepancy in calculations would be accounted for in the real experiment. With a compressor already present in the university, it was considered a very likely possibility that it could be used for the experiment, as it can easily reproduce the pressure and flow requirements. However, due to the extreme pressure ratios that the experiment was to experience, the compressor was ruled out, mainly because of safety and hazardous reasons. Unless the pressure chest was built in a more professional manner to tolerate certain standards of safety, and then officially tested to observe that it withstood these standards, which could be extremely time-consuming, an alternative had to be found to produce the flow. The idea of the utilization of a vacuum pump seemed the most promising method of producing the flow without too much concern, as the pressure ratios could be attained without much danger and the flow could easily be produced. However, vacuum pumps that operate at such a low vacuum level and simultaneously produce a flow of at least 1500 acfm were extremely rare. To find a pump that was also affordable by university standards made the search even more complicated. The search for the ideal vacuum pump went underway, regardless of the rarity of an affordable pump that met the desired requirements. During this time, the experimental setup was still planned with the use of a vacuum pump as the system to produce the flow.

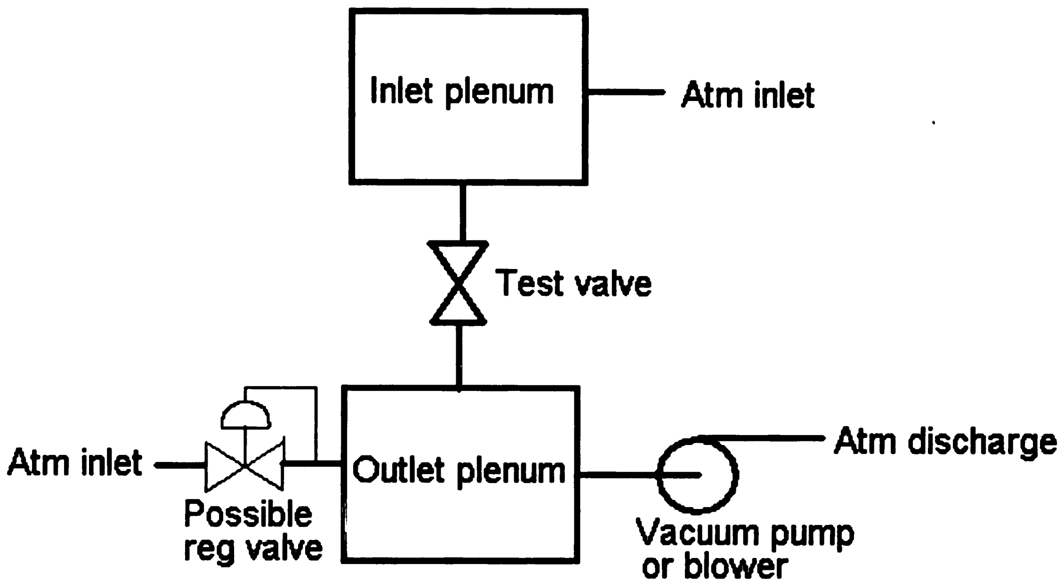

Figure 34: Initial Testing Setup

This was the initial testing plan, without the certainty of a variable speed motor to run the vacuum pump to attain adjustable flow rates and pressure ratios, which makes use of plenums and some regulatory valves and by-pass valves. The basic requirements for the vacuum pump was to be able to attain a high flow of 1500 acfm at a low pressure ratio of 3, of getting a low flow of about 335 acfm at a low pressure ratio of 10, and to be able to regulate the test valve discharge pressure and flow at a high pressure ratio. Varying the pump/blower speed can do this regulation, as well as throttling the pump/blower inlet, or using a by-pass valve. Each possible regulatory method has some issues to them, such as whether the variation of pump/blower speed is adequate to produce a slow flow and whether the slow flow required can be reached to attain the desired pressure ratio. If throttling the inlet was the method to regulate the discharge, is it safe for the machine and can such a low flow be attained with just throttling? Using a by-pass valve requires the checking of any problems if the pumping was done with no load.

Detroit Air Compressor (DAC), a company that supplies vacuum pumps, blowers and compressors, had found the ideal pump that very much met all the above requirements and answered much of the questions above regarding the regulation of flow. The unit is a positive displacement blower, made by ROOTS. The blower is a ROOTS RAM™ Whispair 616 DVJ Dry Vacuum Pump.

4.2.1 The ROOTS RAM™ Whispair 616 DVJ Dry Vacuum Pump

This Whispair dry vacuum pump is a heavy-duty unit with an exclusive discharge jet plenum design that allows cool, atmospheric air to flow into the casing. This unique design permits continuous operation at vacuum levels to blank-off with a single stage unit, without water injection. Standard dry vacuum pumps are limited to approximately 16" Hg vacuum because operation at higher vacuum levels can cause extreme discharge temperatures resulting in casing and impeller distortion. The Roots Whispair vacuum pump's cooling design eliminates the problems caused by high temperatures at vacuum levels beyond 16" Hg. Whispair vacuum pumps reduce noise and power loss by utilizing an exclusive wrap-around plenum and pro-prietary Whispair jet to control pressure equalization, feeding backflow in the direction of impeller movement, aiding rotation. The general statistics of the vacuum pump are shown in the table below.

Frame Size	Speed RPM	Maximum Free Air CFM	12” Hg Vac. CFM at BHP		16” Hg Vac. CFM at BHP		20” Hg Vac. CFM at BHP		24” Hg Vac. CFM at BHP		27”Hg Vac. CFM at BHP	
616J	1750	2367	1015	36	901	47	748	59	448	71	*	80
	2124		1310	44	1196	58	1043	72	743	86	*	97
	2437		1556	51	1443	67	1290	83	990	99	244	111
	3000		2001	63	1887	83	1734	102	1434	122	688	137

Table 7. Performance Table

This pump, with a 100 HP motor, however, cannot produce the desired flow of 1500 acfm. However, looking back at section 2.1.1, the minimum flow required to maintain the pressure of ratio 3 was 25.237 (891.2367) m^3/min (acfm). With a 100 HP motor at a pressure ratio of 3, the vacuum pump can produce a maximum flow of about 1300 acfm. It was also calculated that with this 100 HP motor, the flow produced at a pressure ratio of about 10 would be 54 acfm. It was decided that this pump with a 100 HP motor would suffice for the experiment since at both ends of the operating range of the vacuum pump the flows produced at the required pressure ratios was satisfactory, or at least close enough the to desired values. A powerful motor would reach the desired flow rates and speeds required, but it would require more funds, and the trade-off for spending more funds to obtain just a little more power to meet the desired values was not satisfactory. The performance curves and the performance summary for the vacuum pump operating at the 2 ends of the pressure ratio range of 3 and 10 are shown below.

Gas	Air	Elevation	0 feet
Relative Humidity	36 %	Pressure	14.7 PSIA
Molecular Weight	28.7	Temperature	68 °F
k-Value	1.4	Relative Humidity	36 %
Specific Gravity	0.991		
Ambient Pressure	68 °F		

Table 8. Ambient and Standard Conditions for Vacuum Pump Operation

Actual Volume	400 ACFM
Standard Volume	54 SCFM
System Inlet Pressure	26 inches Hg vacuum
Inlet Pressure Loss	0 PSI
System Discharge Pressure	14.7 PSIA
Discharge Pressure Loss	0 PSI
Inlet Temperature	68 °F

Table 9. Input Conditions for Vacuum Pump Operation for Pressure ratio of 10

Speed	2165 RPM	Jet Volume Flow	899 ACFM
Power at blower shaft	94.9 BHP	Gear tip speed	3404 FPM
Blower differential pressure	12.71 PSI	V-belt Estimated B10 Brg Life	60560 hours
Temperature Rise	236 °F	Coupling Est. B10 Brg Life	571958 hours
Discharge Temperature	304 °F	Est Free Field Noise at 1 meter	96.4 dBa
Discharge volume	1353 ACFM	CFR	0.789
Jet Pressure	14.4 PSIA	Shaft Diameter	2 inches
Jet Temperature	68 °F	Minimum Sheave Diameter	8.5 inches
Jet Weight Flow	64.7 lb/min	Inlet/Discharge Connection	8F/10F/8F (JET)

Table 10. Input Conditions for Vacuum Pump Operation for Pressure ratio of 10

Actual Volume	1284 ACFM
Standard Volume	430 SCFM
System Inlet Pressure	20 inches Hg vacuum
Inlet Pressure Loss	0 PSI
System Discharge Pressure	14.7 PSIA
Discharge Pressure Loss	0 PSI
Inlet Temperature	68 °F

Table 11. Input Conditions for Vacuum Pump Operation for Pressure ratio of 3

Speed	2165 RPM	Coupling Est. B10 Brg Life	1096189 hours
Power at blower shaft	76.9 BHP	Est Free Field Noise at 1 meter	89.6 dBa
Blower differential pressure	9.78 PSI	CFR	0.789
Temperature Rise	35 °F	Shaft Diameter	2 inches
Discharge Temperature	103 °F	Minimum Sheave Diameter	8.5 inches
Discharge volume	458 ACFM	Inlet/Discharge Connection	8F/6F
Water Injection	6 GPM		
Gear tip speed	3404 FPM		
V-belt Estimated B10 Brg Life	116067 hours		

Table 12. Input Conditions for Vacuum Pump Operation for Pressure ratio of 3

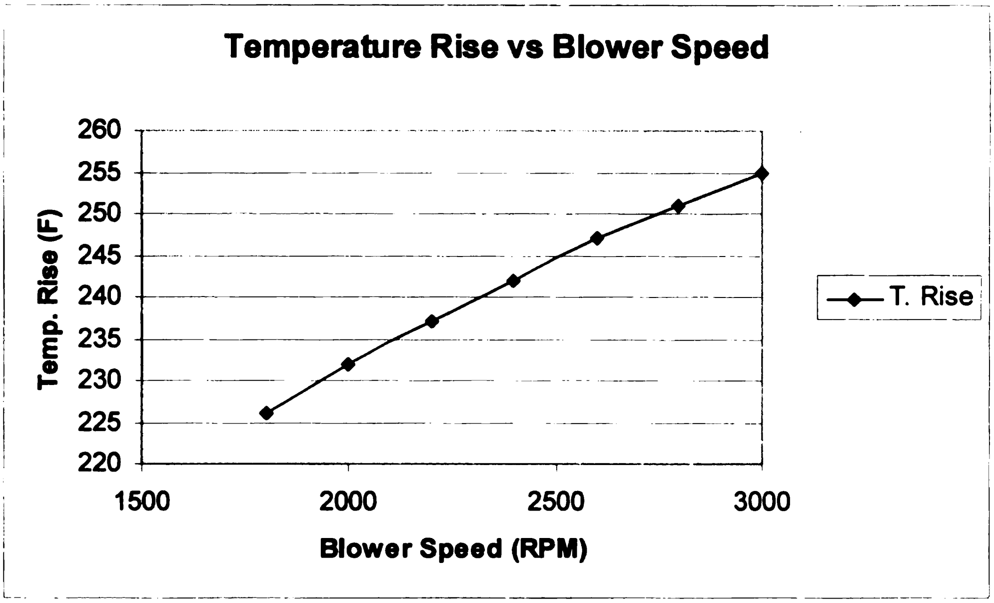

Figure 35: Relationship of Temperature Rise and Blower Speed for Pressure Ratio of 10

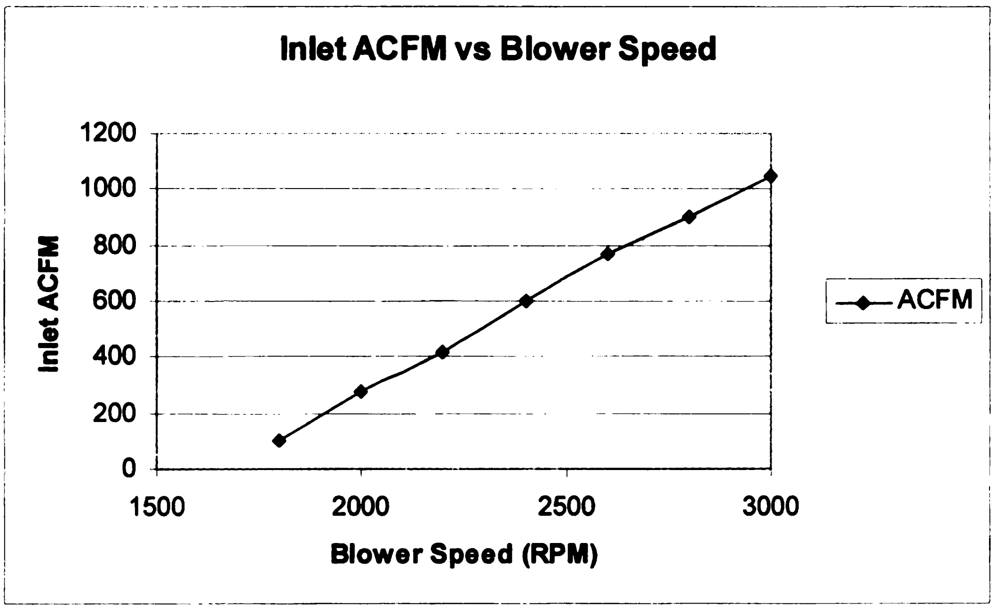

Figure 36: Relationship of Inlet ACFM and Blower Speed for Pressure Ratio of 10

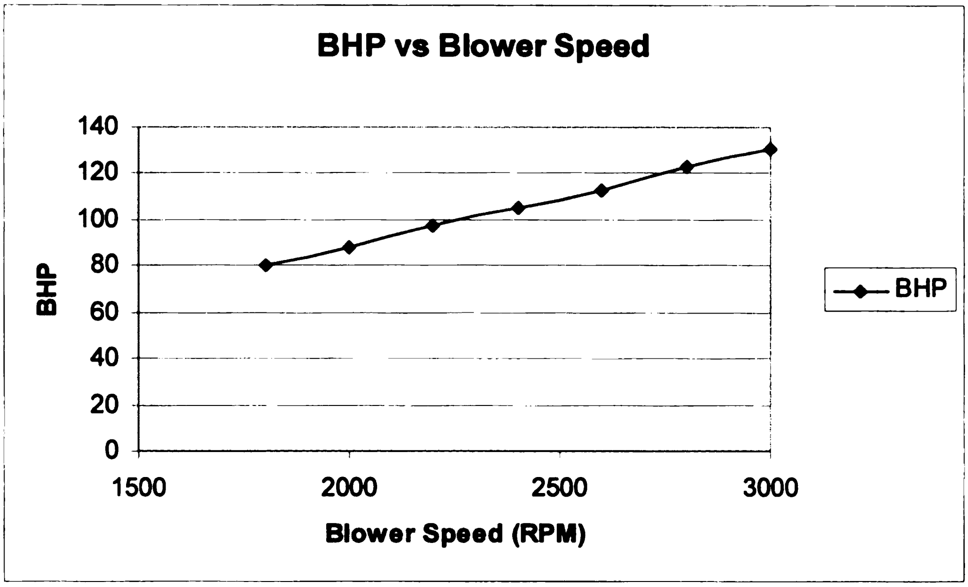

Figure 37: Relationship of Brake Horsepower and Blower Speed for Pressure Ratio of 10

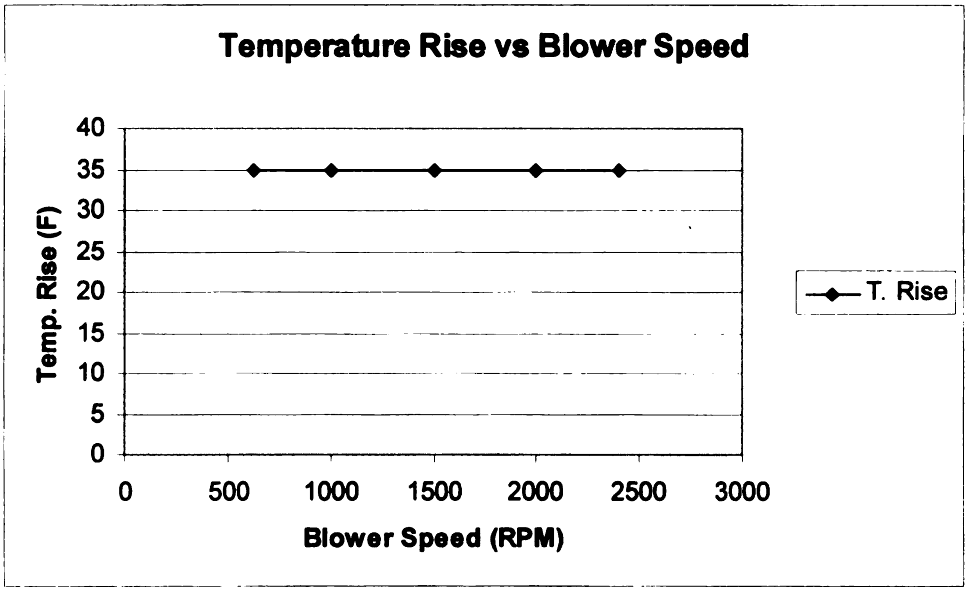

Figure 38: Relationship of Temperature Rise and Blower Speed for Pressure Ratio of 3

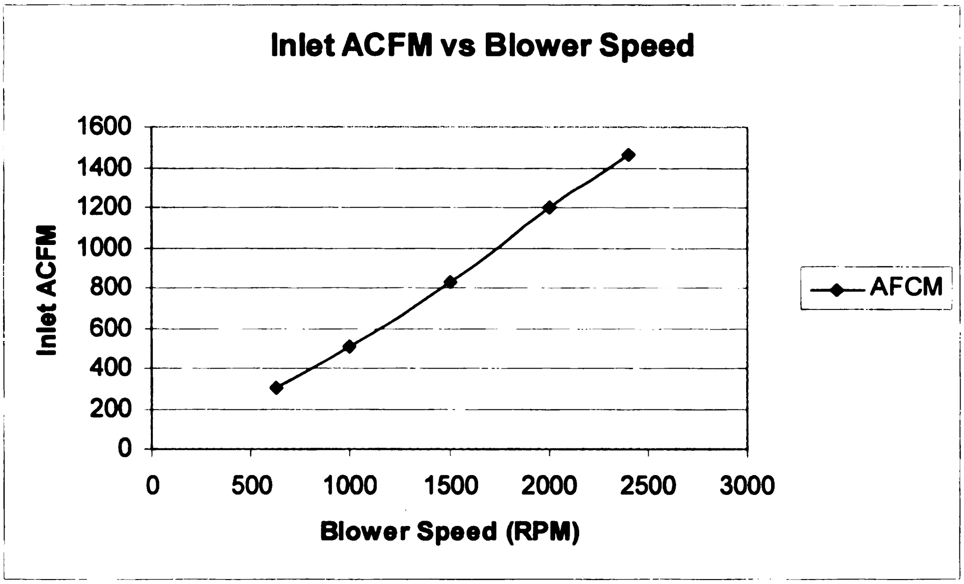

Figure 39: Relationship of Inlet ACFM and Blower Speed for Pressure Ratio of 3

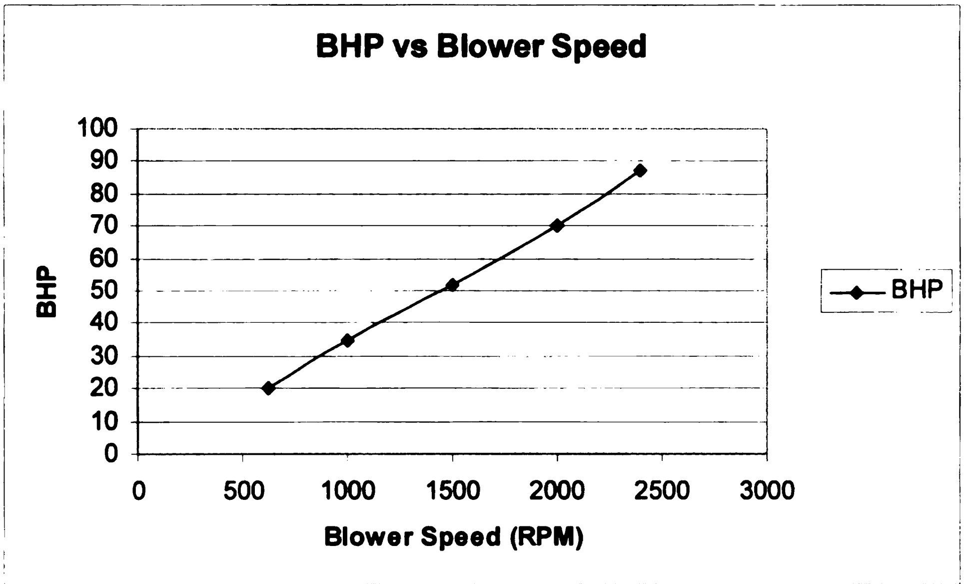

Figure 40: Relationship of Brake Horsepower and Blower Speed for Pressure Ratio of 3

The entire vacuum pump package includes the ROOTS RAM™ Whispair 616 DVJ Dry Vacuum Pump mounted on a Stoddard D93 10X8 combination inlet and discharge silencer. The vacuum pump is belt-driven, enclosed by an OSHA belt guard, with a 100 Horsepower 1800-RPM TEFC 3/60/230 460-volt motor. Looking at the initial setup, varying the flow could be done by either varying the pump/blower speed, throttling the pump/blower inlet, or using a by-pass valve. However, there were some concerns for each method for regulating the flow. Using the bypass valve would draw in a tremendous amount of flow and may increase the noise during operation. The simplest method of varying the flow speed would be to vary the motor speed, which can be done using a variable-speed motor. However, the purchase of a variable-speed motor increases the price of the overall vacuum pump. Throttling the inlet would work without too much concern for the operation of the pump because of the jet discharge. Since the motor can only run at one speed, and hence provide a fixed flow rate through the overall system, throttling the inlet would decrease the flow through the test valve. However, the rest of the flow to fulfill the fixed flow rate can be drawn through the jet silencer. A reticulation valve could also work, but it might overheat as the lift of the valve increases. Even at low flows at high pressure ratios, the motor could provide a 54 SCFM, but that is at the maximum power from the motor. A bypass valve to draw in more air into the inlet would be beneficial, as the motor would not have to run at maximum capacity, and hence prevent a possible overheat. It would have to be drawn from upstream of the flow-measuring orifice, so the bypass flow would not be counted in the flow measurement. The capabilities of the vacuum pump to produce the flow at the opposite ends of the pressure range are mapped on this figure to observe the accuracy of the model valve to the actual valve.

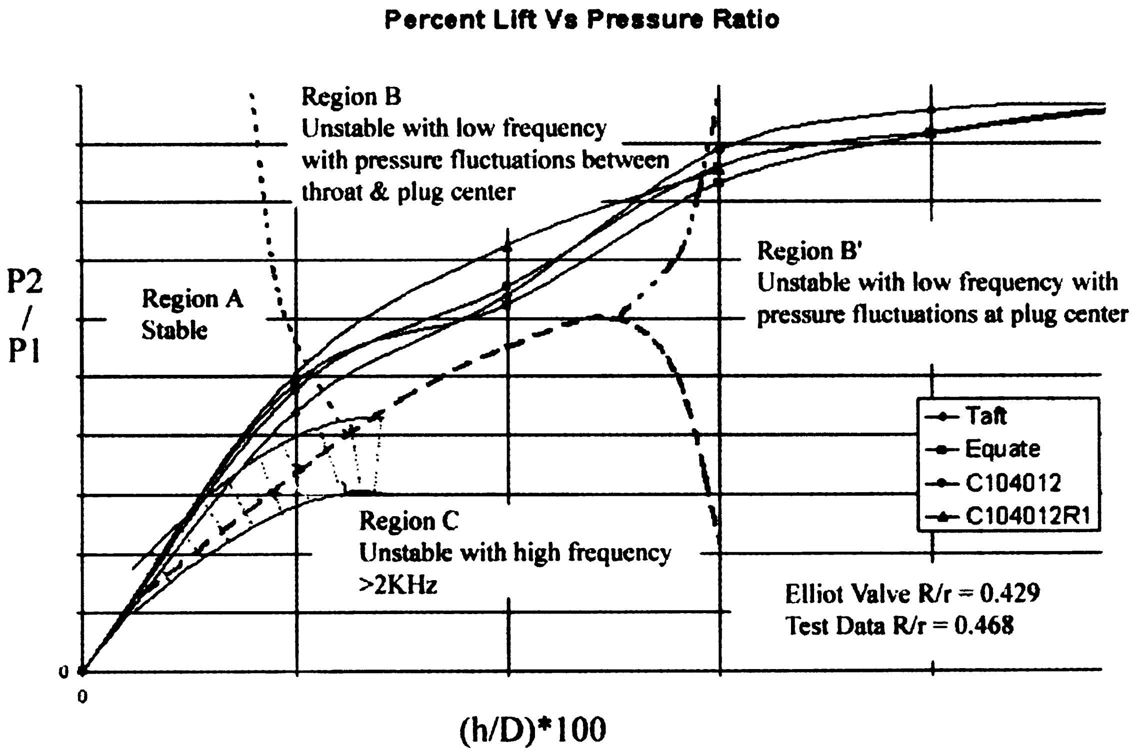

Figure 41: Flow Pattern of Valves
(Source: Elliot Turbo-Machinery Co., 2001)

Appendix A
Profiles for the 0.4595 and 0.639 Inch Lifts

Profiles for 0.4595 Inch Lift

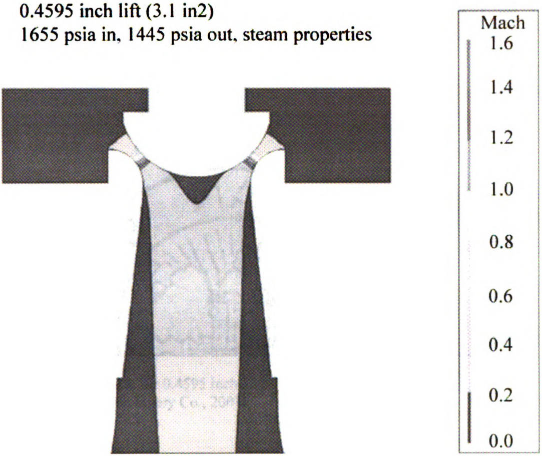

Figure 42: Mach Number Profile for 0.4595 inch Lift
(Source: Elliot Turbo-Machinery Co., 2001)

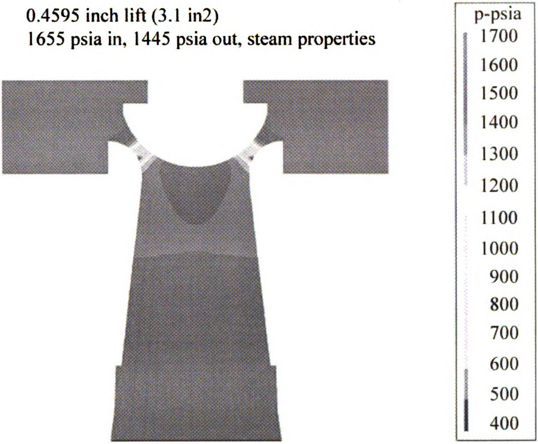

Figure 43: Pressure Profile for 0.4595 inch Lift
(Source: Elliot Turbo-Machinery Co., 2001)

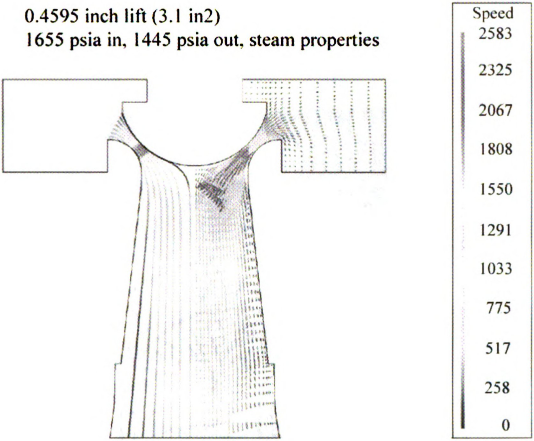

Figure 44: Velocity Profile for 0.4595 inch Lift
(Source: Elliot Turbo-Machinery Co., 2001)

Profiles for 0.639 Inch Lift

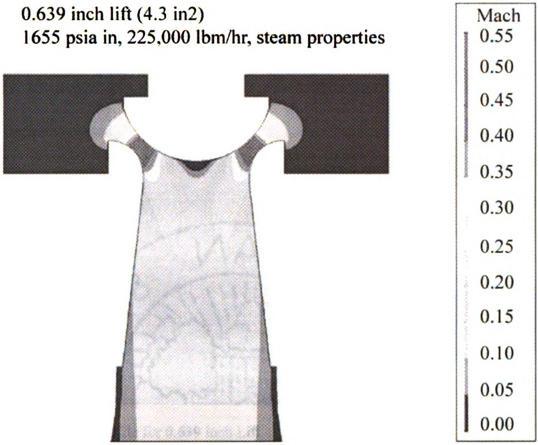

Figure 45: Mach Number Profile for 0.639 inch Lift
(Source: Elliot Turbo-Machinery Co., 2001)

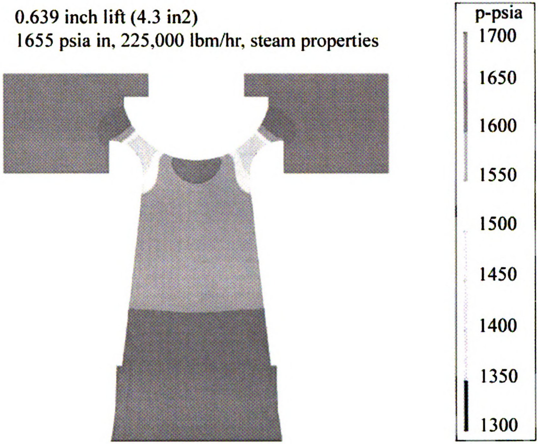

Figure 46: Pressure Profile for 0.639 inch Lift
(Source: Elliot Turbo-Machinery Co., 2001)

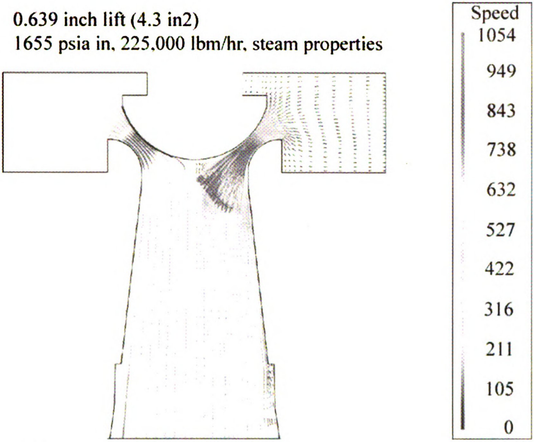

Figure 47: Velocity Profile for 0.639 inch Lift
(Source: Elliot Turbo-Machinery Co., 2001)

Appendix B
Pressure Chest and Valve Design Dimensions

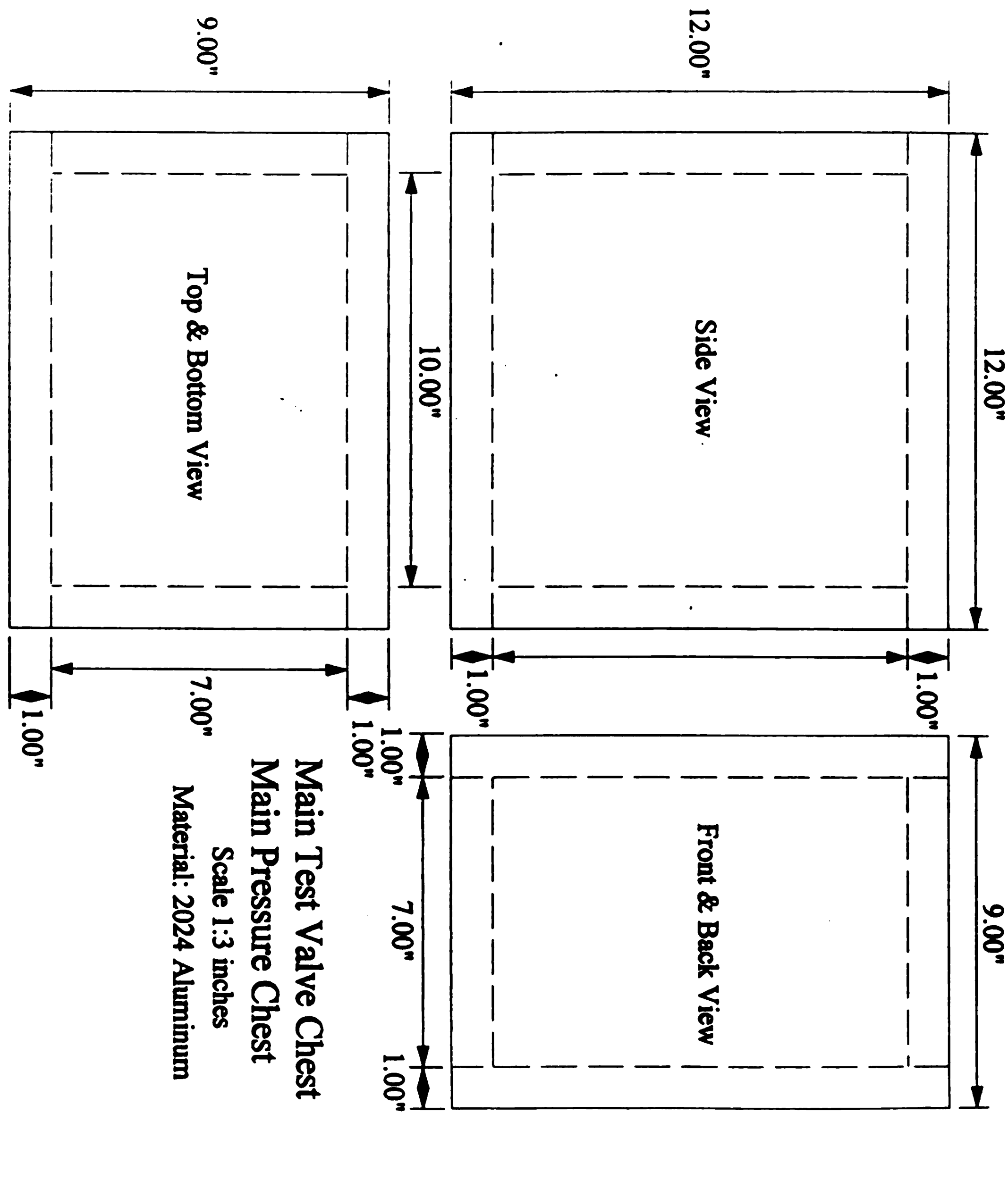

Figure 48: Main Testing Valve Pressure Chest

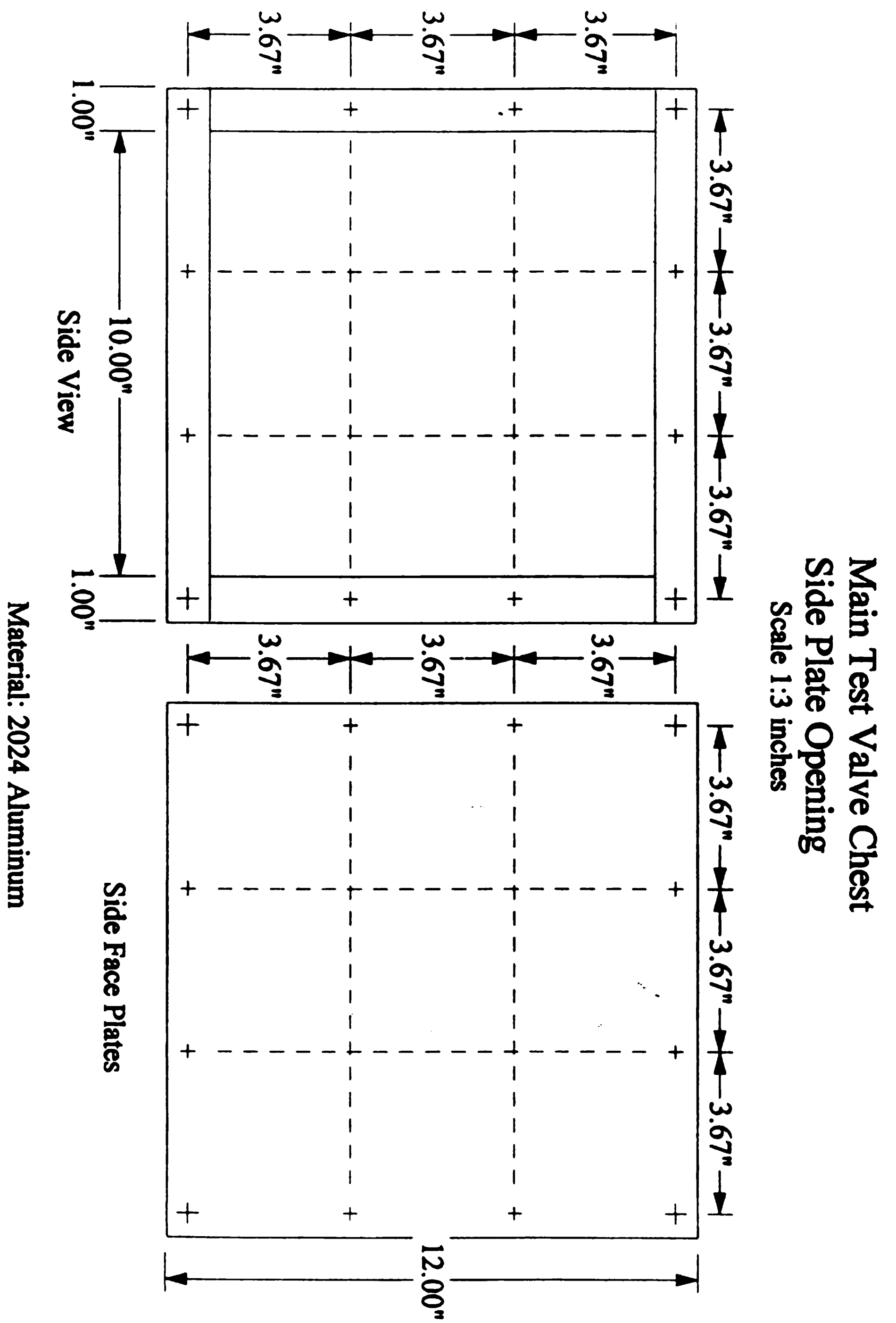

Figure 49: Side Plating Dimensions for Pressure Chest Opening

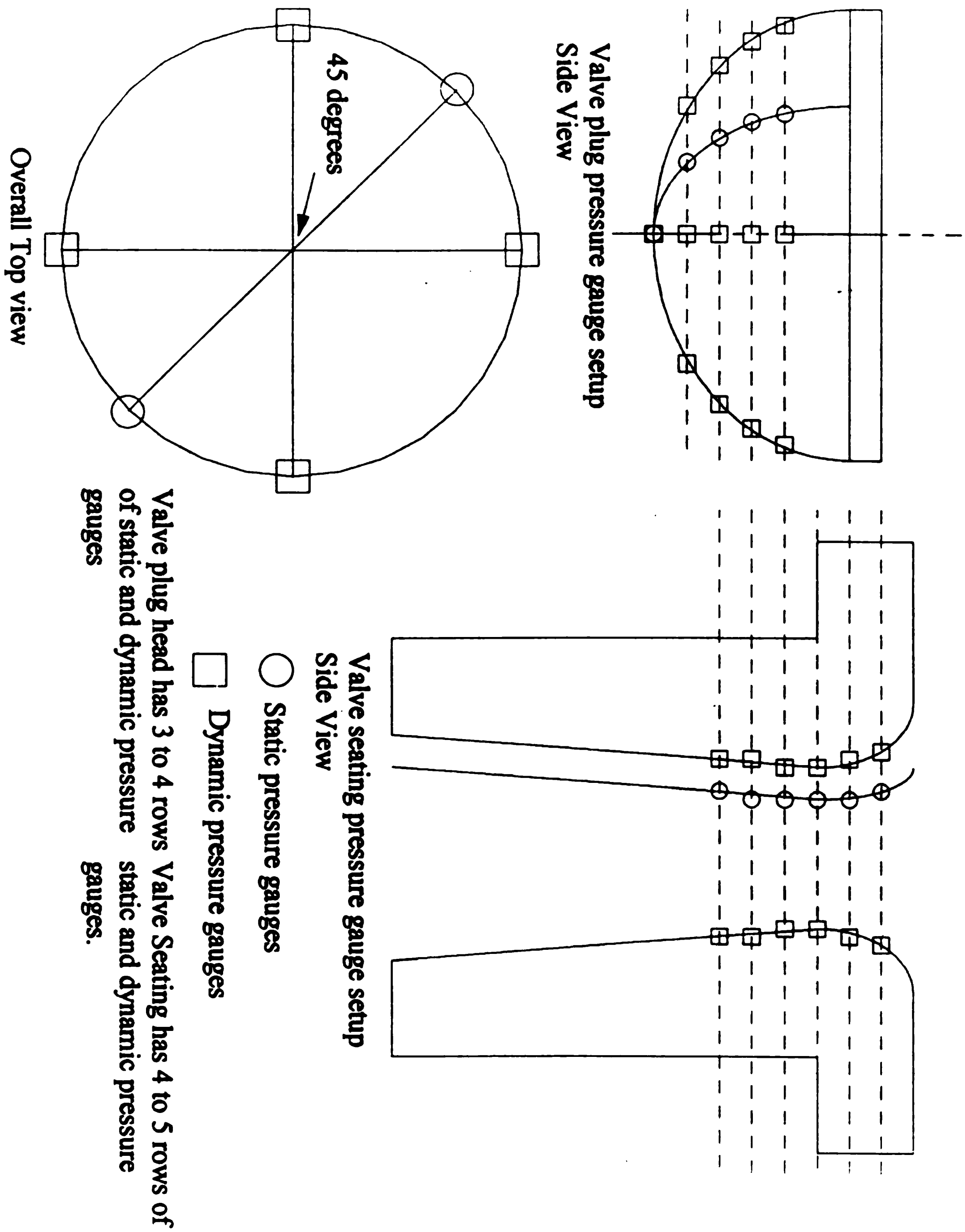

Figure 50: Valve and Seating Pressure Gauge Arrangement

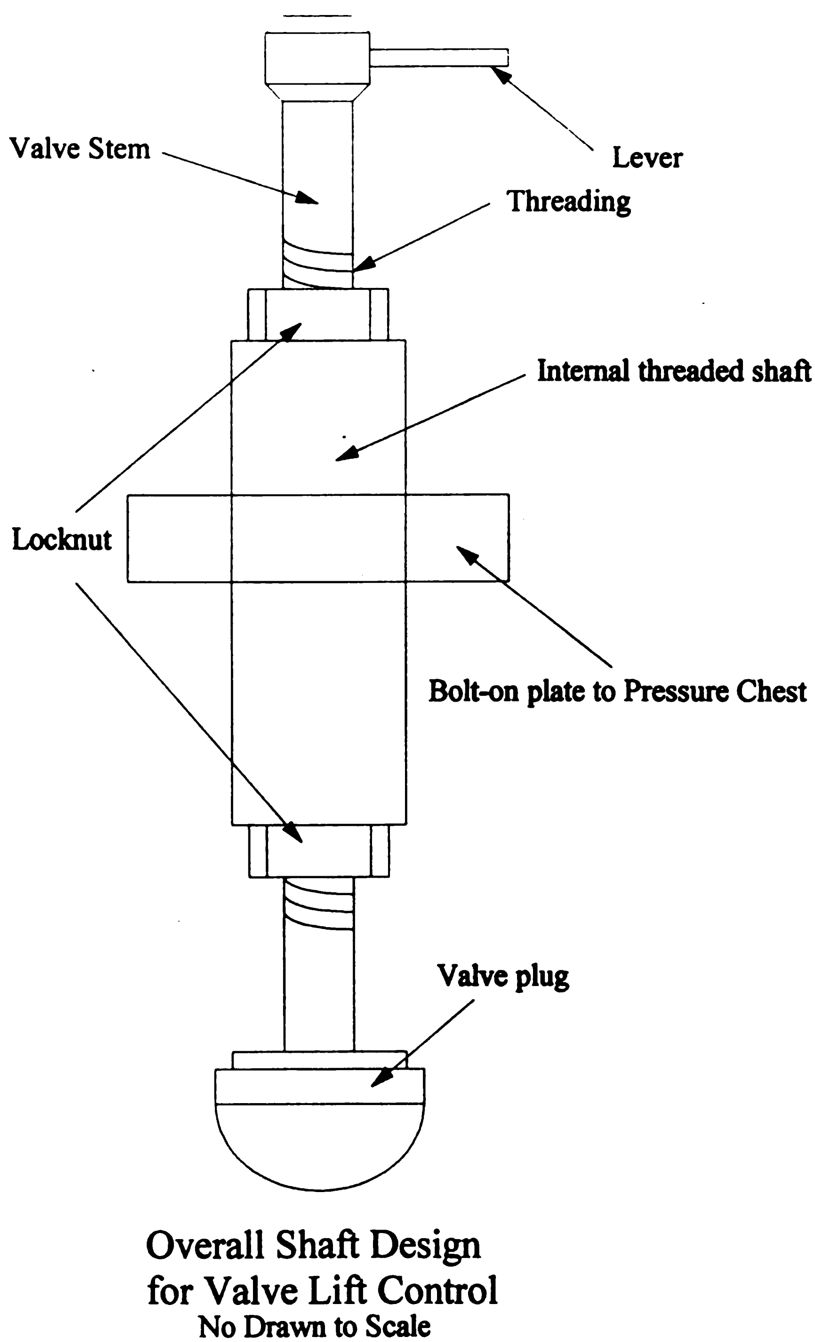

Figure 51: Overall Shaft Design for Valve Lift

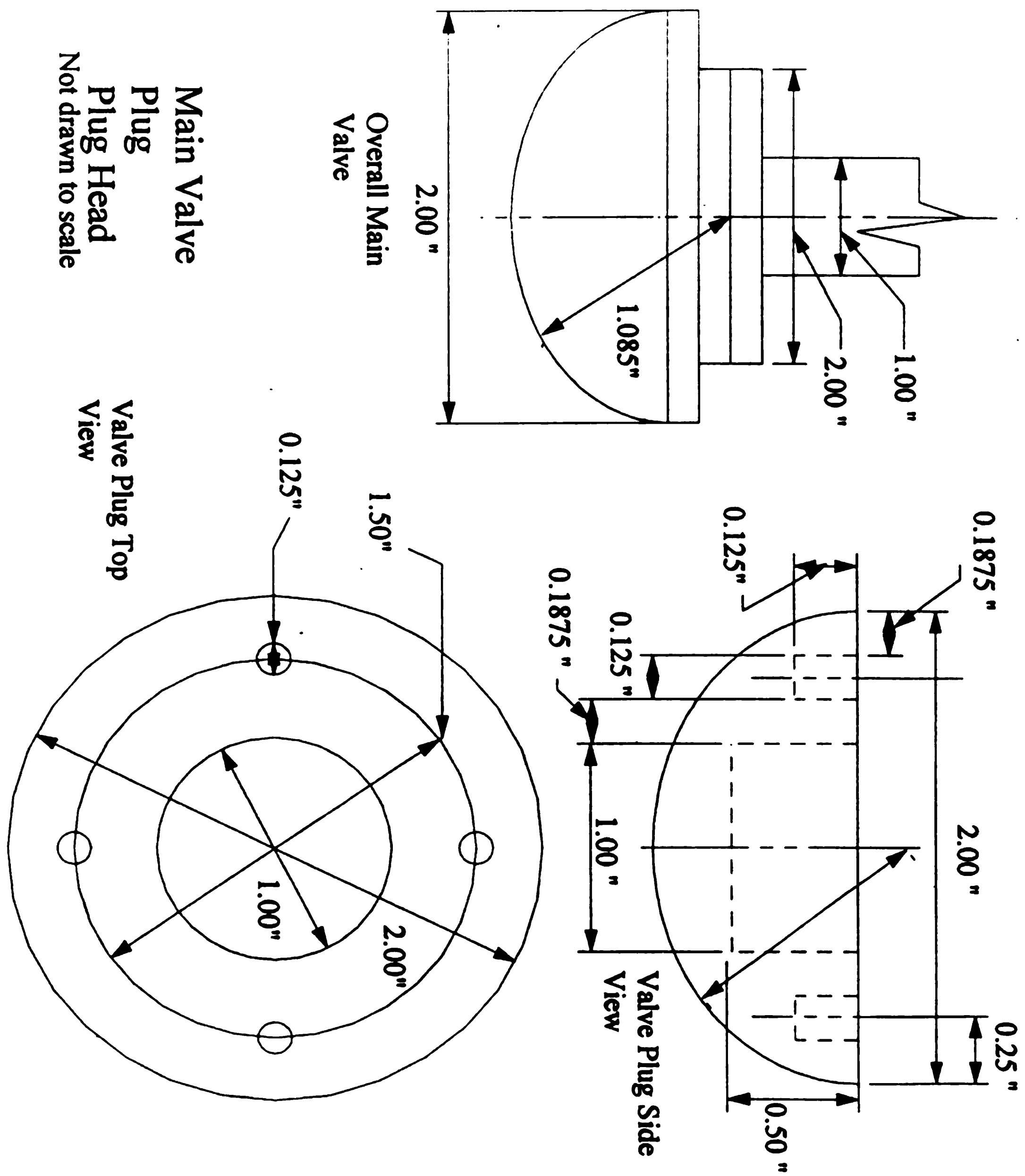

Figure 52: Dimensions for Main Valve Plug Head

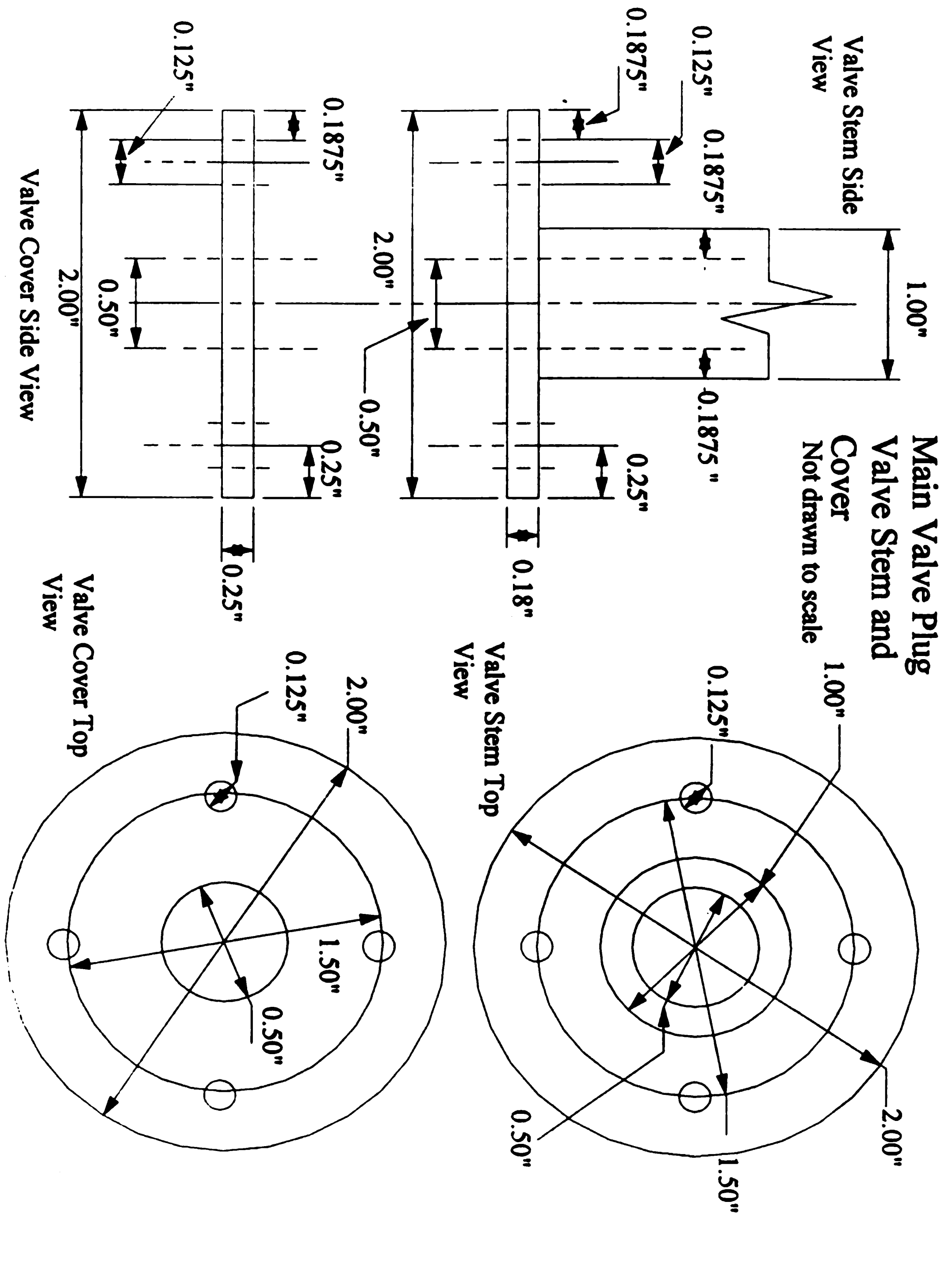

Figure 53: Dimensions for Valve Stem and Plate Bolt On

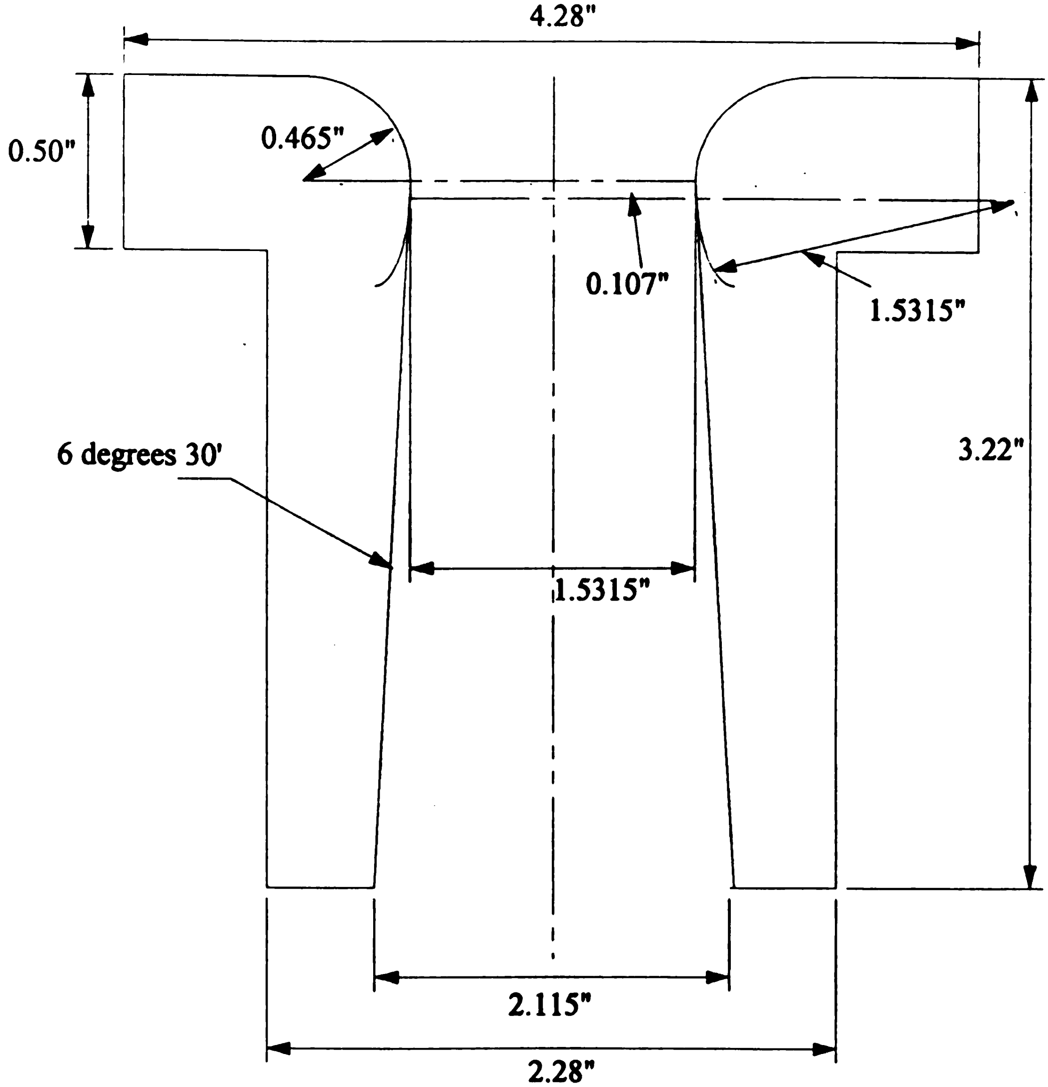

Main Valve Design and Seating
Not drawn to scale

Figure 54: Dimensions for Main Valve Seating

Appendix C
Aluminum 2024-T851

Subcategory: Aluminum Alloy; Nonferrous Metal; 2000 Series Aluminum Alloy

Key Words: Aluminum 2024-T851; AA2024-T851; UNS A92024;

Composition:

COMPONENT	WT. %
AL	93.5
CR	MAX 0.1
CU	3.8 - 4.9
COMPONENT	WT. %
FE	MAX 0.5
MG	1.2 - 1.8
MN	0.3 - 0.9
COMPONENT	WT. %
SI	MAX 0.5
TI	MAX 0.15
ZN	MAX 0.25

Table 13. Composition Table for aluminum 2024

Material Notes: Weldability = C; Stress Corrosion Cracking Resistance = B; General Corrosion Resistance = D (A = best; E = worst). Good machinability and surface finish capabilities. A high strength material of adequate workability. Has largely superceded 2017 for structural applications.

Uses: Aircraft fittings, gears and shafts, bolts, clock parts, computer parts, couplings, fuse parts, hydraulic valve bodies, missile parts, munitions, nuts, pistons, rectifier parts, worm gears, fastening devices, veterinary and orthopedic equipment, structures.

Most data provided by Alcoa.

PHYSICAL PROPERTIES	VALUES	COMMENTS	US / Other Units
Density, g/cc	2.77		2.77 g/cc
Hardness, Brinell	128	500 kg load/10 mm ball	128
Hardness, Knoop	161	Estimated from Brinell	161
Hardness, Rockwell A	49	Estimated from Brinell	49
Hardness, Rockwell B	79	Estimated from Brinell	79
Hardness, Vickers	146	Estimated from Brinell	146

Table 14. Physical Properties of Aluminum 2024

MECHANICAL PROPERTIES	VALUES	COMMENTS	US / Other Units
Tensile Strength, Ultimate, MPa	455	Minimum value	65,975 psi
Tensile Strength, Yield, MPa	400	Minimum Value	58,000 psi
Elongation %; break	5		5 %
Modulus of Elasticity, GPa	72.4	Estimated from other heat treatments.	10,498 ksi
Poissons Ratio	0.33	Estimated from other heat treatments.	0.33
Fatigue Strength, MPa	117	500,000,000 cycles; completely reversed; R. R. Moore Machine and specimen.	16,965 psi
Machinability, %	70	0-100 Scale (A=90; B=70; C=50; D=30; E=10)	70
Shear Modulus, GPa	27	Estimated from similar Al alloys.	3,915 ksi
Shear Strength, MPa	296		42,920 psi

Table 15. Mechanical Properties of Aluminum 2024

THERMAL PROPERTIES	VALUES	COMMENTS	US / Other Units
CTE, linear 20°C, µm/m-°C	23.2	average over 20-100°C	13 µin/in-°F
CTE, linear 250°C, µm/m-°C	24.7	Average over the range 20-300°C	14 µin/in-°F
Heat Capacity, J/g-°C	0.875		0.21 BTU/lb-°F
Thermal Conductivity, W/m-K	151		1,048 BTU-in/hr-ft²-°F
Melting Point, °C	502	Solidus	936 °F
Solidus, °C	502		936 °F
ELECTRICAL PROPERTIES	VALUES	COMMENTS	US / Other Units
Electrical Resistivity, Ohm-cm	0.0000045		0.0000045 Ohm-cm

Table 16. Thermal Properties of Aluminum 2024

BIBLIOGRAPHY

Bibliography

1) Schuder, Charles B., "Understanding Fluid Forces in Control Valves", Intrumentaional Technology, Journal of the Instrument Society of America, May 1971

2) Zarjankin, A.; Simonov, B., "New Control Valves, Their Parameters and Service Experience in the Turbines", Joint- Stock Company for the Development of New Technologies in Energetics, ENTEK, Co. Ltd., Russia

3) Araki, Tatsuo; Okamoto, Yasuo; Ootomo, Fumio, "Fluid Induced Vibration of Steam Control Valves",Research and Development UDC 534.11.001.5:621.165-3

4) Eguchi, Tsuyoshi; Hirota, Kazuo; Honjo, Masanobu; Magoshi, Ryotaro, "Study of Self-Excited Vibration of Governing Valves for Large Steam Turbines", Mitsubishi Heavy Industries, Ltd

5) Cengal, Yunus A.; Boles, Nichael A., "An Engineering Approach: Thermodynamics", Second Edition, McGraw-Hill, Inc. 1994

6) Halliday, David; Resnick, Robert; Walker, Jearl, "Fundamentals of Physics Extended", Fourth Edition, John Wiley & Sons, Inc. 1993